Dual roles of the plasma membrane calcium ATPases for presynaptic Ca^{2+} homeostasis and the modulation of H^{+} gradient in synaptic vesicles

DOCTORAL DISSERTATION

A thesis submitted in partial fulfillment of the requirements

for the degree of Doctor of Philosophy

By:

Yoshiyasu Ono

Supervisor:

Shigeo Takamori

Graduate School of Brain Science

Doshisha University

September 2019

Kyoto, Japan

Table of contents

Abbreviations

AO	Acridine orange
AP	Action potential
Baf	Bafilomycin
CCP	Clathrin-coated pits
CME	Clathrin-mediated endocytosis
CPA	Cyclopiazonic acid
CSP	Cysteine string protein
DC	Divalent cation
ΔpH	pH gradient across the synaptic vesicle membrane
$\Delta\psi$	Membrane potential across the synaptic vesicle membrane
$\Delta\mu_{H+}$	Proton electrochemical gradient
G-protein	GTP-binding protein
K & R	Kiss-and-run
IR	Ionotropic receptor
LEV	Levetiracetam
LP2	Crude SV fraction, lysate pellet 2
NT	Neurotransmitter
Q_{10}	Temperature co-efficient
RIM	Rab3-interacting molecule
PMCA	Plasma membrane Ca^{2+} ATPase
SERCA	Sarcoplasmic endoplasmic reticulum
SEP	Super-ecliptic pHluorin
SNARE	Soluble NSF attachment protein receptor

SV	Synaptic vesicle
SV2	Synaptic vesicle-associated glycoprotein 2
SypHy	Synaptophysin-super-ecliptic pHluorin
TeNT	Tetanus toxin
VAChT	Vesicular acetylcholine transporter
VAMP	vesicle-associated membrane protein, synaptobrevin
V-ATPase	Vacuolar-type H^+-ATPase
VGAT	Vesicular GABA transporter
VGLUT	Vesicular glutamate transporter
VMAT	Vesicular monoamine transporter
VNT	Vesicular neurotransmitter transporter
VNUT	Vesicular nucleotide transporter

List of Figures and a Table

Abstract

Ca^{2+} transport into synaptic vesicles (SVs) at the presynaptic terminals has been proposed to be an important process for regulating presynaptic [Ca^{2+}] during stimulation as well as at rest. However, the molecular identity of the transport system remains elusive. Previous studies have demonstrated that isolated SVs exhibit two distinct Ca^{2+} transport systems depending on extra-vesicular (cytosolic) pH; one is mediated by a high affinity Ca^{2+} transporter which is active at neutral pH and the other is mediated by a low affinity Ca^{2+}/H^{+} antiporter which is maximally active at alkaline pH of 8.5. In addition, synaptic vesicle glycoprotein 2s (SV2s), one of the major SV components, have also been proposed to contribute to Ca^{2+} clearance from the presynaptic cytoplasm, although Ca^{2+} transport activity conferred by SV2s has never been demonstrated directly.

In this thesis, I show that, at physiological pH, the plasma membrane Ca^{2+} ATPases (PMCAs) are responsible for both the Ca^{2+}/H^{+} exchange activity and Ca^{2+} uptake into SVs. The Ca^{2+}/H^{+} exchange activity monitored by acidification assay exhibited high affinity for Ca^{2+} (K_m ~ 400 nM) and characteristic divalent cation selectivity for the PMCAs. Both activities were remarkably reduced by PMCA blockers, but not by a blocker of the ATPase that transfers Ca^{2+} from the cytosol to the lumen of sarcoplasmic endoplasmic reticulum (SERCA) at physiological pH. Furthermore, I rule out the contribution of SV2s, putative Ca^{2+} transporters on SVs, since both Ca^{2+}/H^{+} exchange activity and Ca^{2+} transport were unaffected in isolated vesicles derived from SV2-deficient brains.

Finally, using a PMCA1-pHluorin construct that enabled us to monitor cellular distribution

and recycling properties in living neurons, I demonstrated that PMCA1-pHluorin localized to intracellular acidic compartments and recycled at presynaptic terminals in an activity-dependent manner. In addition to the well-known function of plasma membrane PMCAs for Ca^{2+} homeostasis in the presynaptic cytoplasm, my results collectively imply that vesicular PMCAs may play pivotal roles in both presynaptic Ca^{2+} homeostasis and the modulation of H^{+} gradient in SVs.

1. Introduction

1.1 Synaptic transmission

Neural networks consisting of neurons govern all brain functions such as sensory cognition, motor control, emotion, learning and memory. A single neuron is composed of three major compartments: a *cell body*, where the nucleus, protein synthesis machinery and several other organelles are located, *dendrites*, which provide a large surface to receive synaptic inputs from other nerve cells by forming extensive branches called '*dendritic trees*', and *axons*, which are long processes built to conduct nerve impulses from the cell body to the other nerve cells. Axonal branches possess morphologically distinct regions called *boutons*, which are club-shaped enlargements attached very close to the cell bodies or to the dendrites of other neurons. The place of close contact between two neurons where the neuronal signals are transmitted is called "*synapse*", and the narrow space between the two neurons is called the *synaptic cleft*. Synapses are classified broadly into two types based on their mechanism of transmission: electrical synapses and chemical synapses. At the electrical synapses, the two communicating neurons are linked together by *gap junctions*, which consist of precisely aligned channels of the two neurons [1]. On the other hand, at chemical synapses, the information is transmitted via release of chemical signals called *neurotransmitters* from the presynaptic neuron to postsynaptic neurons through the synaptic clefts (Figure 1-1a). Prior to release, the neurotransmitter molecules are stored in spherical, membrane-bound organelles called *synaptic vesicles* (*SVs*) (Figure 1-1). The principal feature of chemical synapses, which are the most abundant type of synapse in the nervous system, is the accumulation of synaptic vesicles near the presynaptic membrane (Figure 1-1b).

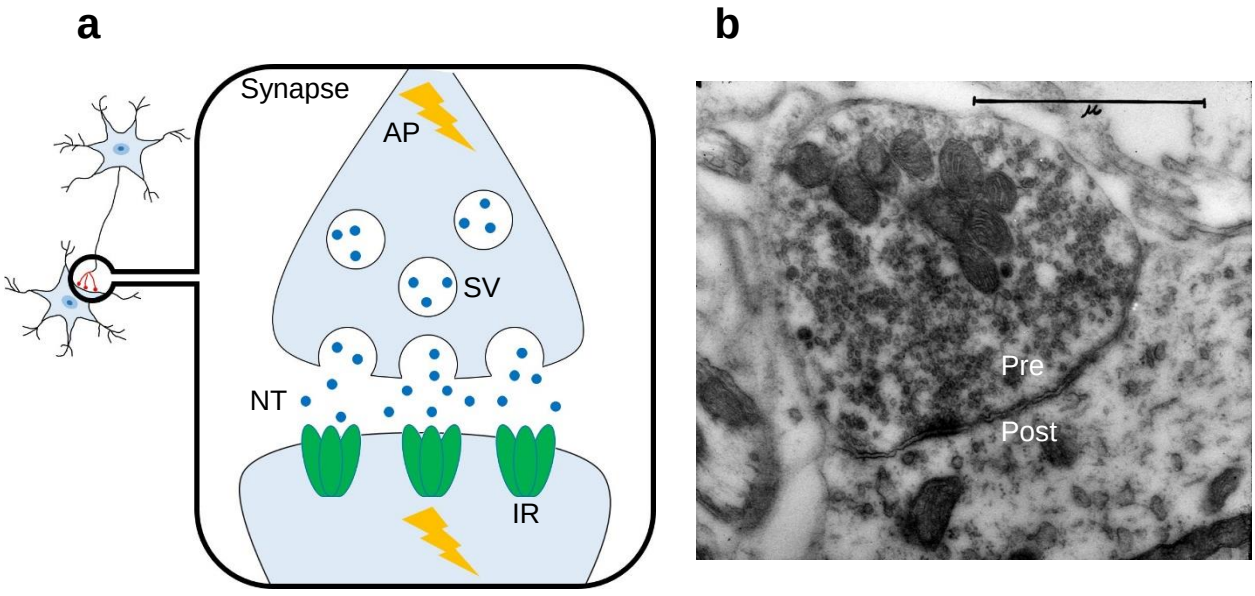

Figure 1-1 Characteristics of the chemical synapse.

(a) Schematic representation of the mechanism of the synaptic transmission. The red part of the left picture shows the synapse, and the right picture is the enlarged figure of the synapse. The neurotransmitters (NTs) are loaded into synaptic vesicles (SVs), and are released to the synaptic cleft upon the arrival of an action potential (AP). Then, the ionotropic receptors (IR) at the postsynaptic cells are activated by the neurotransmitters, leading to alterations of the postsynaptic membrane potential.

(b) An electron micrograph of a synapse. The small black particles at the presynaptic cell are synaptic vesicles. Modified from the picture of the website: http://whitney.med.yale.edu/gsdl/cgi-bin/library?c=palade&a=d&d=DpaladeNerJ.

The sequence of events involved in synaptic transmission at a chemical synapse occurs as follows: First, a nerve impulse in the form of a brief electrical discharge, called an *action potential* (*AP*), invades the presynaptic bouton, and depolarizes the presynaptic membrane. The membrane

depolarization causes an opening of voltage-dependent Ca^{2+} channels at the presynaptic plasma membrane, resulting in an elevation of presynaptic Ca^{2+} concentrations by an influx of extracellular Ca^{2+}. This triggers SVs to fuse with the presynaptic membrane, a process called *exocytosis*, which leads to release of their neurotransmitter contents into the synaptic cleft. Then, the neurotransmitter molecules diffuse across the synaptic cleft and bind to specific receptors at the postsynaptic membrane (Figure 1-1). There are two types of postsynaptic receptors, which differ in their structures and mechanisms by which neurotransmitter biding is translated into the postsynaptic responses. One type is the *ionotropic receptors*, which contain membrane-spanning domains that form an ion channel (Figure 1-1). The other type is the metabotropic receptors, which do not have an ion channel structure. Instead, neurotransmitter binding to these receptors activates intermediate molecules called *G-proteins* (*GTP-binding proteins*), which interact either directly with ion channels or with other effector proteins, such as phospholipase C, that regulate ion channels or other signaling pathways.

1.2 Quantal hypothesis of neurotransmitter release

One of the most prominent features in neurotransmitter release is their quantal nature. Pioneering work by Katz and colleagues in early 1950s, accompanied by the realization of clusters of homogeneously sized membrane sacs at the presynaptic terminals (Figure 1-1b)[2], proposed that neurotransmitters are released as a shape of quantal packets of neurotransmitters that are stored in synaptic vesicles [3,4]. The amount of neurotransmitter released from a presynaptic terminal is determined by the number of available vesicles, the probability of the available vesicles to be released and the amount of neurotransmitters

in a vesicle. The strength of neurotransmission, which can be measured electrophysiologically as postsynaptic currents (PSCs), can be therefore described as the product of these parameters;

$$PSCs = N \times P_r \times q$$

where N, Pr, and q represent the number of release sites (or number of vesicles available for release), release probability and quantal size, respectively. The quantal size is essentially defined by both the amount of neurotransmitters from a single vesicle and the sensitivity of postsynaptic receptors. Although the original quantal hypothesis predicted that the amount of neurotransmitters in a single vesicle is constant, various presynaptic factors are currently known to modulate the amount of neurotransmitters [5] (see 1.3.3 for detail).

1.3 Synaptic vesicle recycling

At presynaptic terminals, Ca^{2+}-triggered SV exocytosis is followed by recapture and reuse of presynaptic membranes to form new SVs, which is called *endocytosis*. The newly formed SVs are then re-acidified by the activity of the *vacuolar-type H^+-ATPase* (*V-ATPase*) and are loaded with neurotransmitters for the next round of exocytosis. This trafficking cycle is called *synaptic vesicle recycling*, which enables the synapse to sustain neurotransmission particularly in response to high-intensity synaptic inputs [6]. As described, one complete round of SV recycling has three steps: exocytosis, endocytosis, and neurotransmitter loading (Figure 1-2). To fulfill the complete synaptic vesicle recycling, SVs must be equipped with variety of proteins, including proteins required for membrane trafficking and fusion, a Ca^{2+} sensor that triggers Ca^{2+}-dependent rapid

fusion of SVs to the plasma membrane, and proteins required for neurotransmitter uptake. Since SVs are the smallest organelle with limited space (approximately 40 nm in diameter) and it is feasible to obtain biochemically amenable amount from native mammalian brains, SVs are one of the best-characterized organelle at molecular levels [7]. Since late 1980s, intensive work has been made to identify key components in SV functions. Biochemical analysis of each component as well as interactions with other components has revealed protein complexes that are required for particular processes. Furthermore, identification of genes encoding SV proteins allowed us to generate animal models which essentially lacked individual genes. Morphological, biochemical and physiological assessments of neural preparations or SV preparations from such animals have deepened our knowledge on molecular mechanisms of neurotransmitter release.

In the following sections, I will briefly describe our current knowledge of each step and underlying molecular mechanisms.

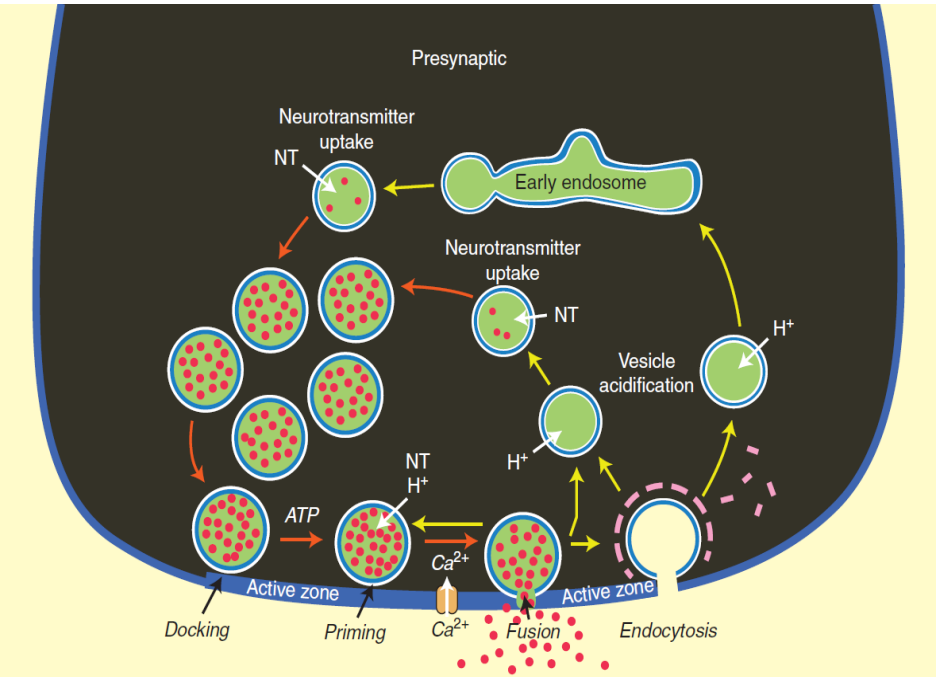

Figure 1-2 The synaptic vesicle cycle.

The information is transferred via release of neurotransmitter molecules (NT; red dots) stored in SVs (green circles) at the presynaptic terminal. The neurotransmitters are loaded into SVs by cooperation of several SV proteins among which the V-ATPase and the vesicular neurotransmitter transporters play the main role. SVs filled with the neurotransmitters are translocated to the active zones (the blue thick region) where SV docking and priming occur. Upon arrival of an AP, voltage-dependent Ca^{2+} channels open, which in turn results in an increase in the concentration of Ca^{2+} at the active zones. Then, the Ca^{2+} increment triggers fusion of the SV membrane with the presynaptic membrane, causing the release of their contents. The release occurs via either a transient fusion pore (kiss and run) or a full collapse of SVs into the presynaptic membrane. After exocytosis, SV membranes and their constituents are recaptured from the presynaptic membrane via clathrin (dashed pink line)-mediated endocytosis. After clathrin uncoating, SVs are regenerated in the nerve terminal, which probably involves membrane trafficking through a presynaptic endosomal compartment. Red arrows indicate processes to achieve exocytosis, whereas yellow arrows show multiple modes of endocytosis and the subsequent vesicle regeneration process. . Modified from Südhof and Rizo, 2011 [8].

1.3.1 Exocytosis

Exocytosis is composed of three distinct steps: vesicle docking, vesicle priming, and vesicle fusion. *Vesicle docking* is a process in which synaptic vesicles are physically docked with plasma membranes. In this process, *RIMs* (*Rab3-interacting molecules*) localized at active zones [9] are thought to play a key role (Figure 1-3). These proteins also bind to small GTPases, such as *Rab3* and *Rab27,* which are localized on SVs [10] as indicated in Figure 1-3 and Figure 1-4, thereby tethering SVs to the active zone.

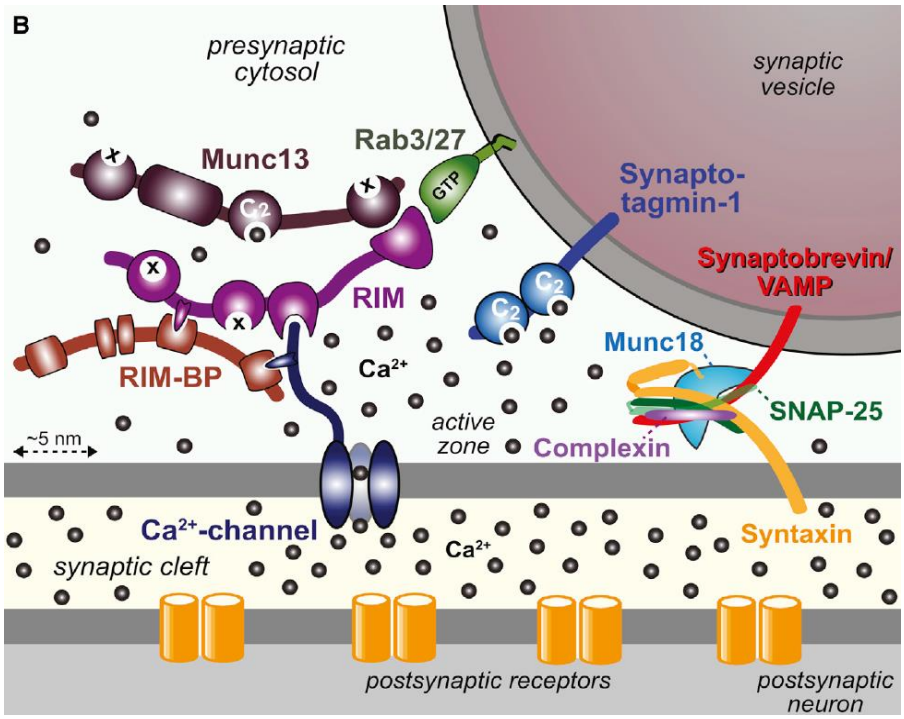

Figure 1-3 Molecular organization of the presynaptic release machinery.

A schematic drawing of the molecular machinery mediating Ca^{2+}-triggered SV exocytosis. The drawing depicts a part of a docked synaptic vesicle on the top right and the presynaptic active zone in the middle. The three functional elements of the neurotransmitter release machinery are depicted from right to left. On the right, the core fusion machine composed of the SNARE/Munc 18 protein complex is shown; this machine comprises the SNARE proteins synaptobrevin/VAMP, syntaxin-1, and SNAP-25 and Munc18-1. The Ca^{2+} sensor synaptotagmin-1 is depicted in the middle; it is composed of a short intravesicular sequence, a single transmembrane region, and two cytoplasmic C2 domains that bind Ca^{2+}, and it functions using complexin (bound to the SNARE complex) as its cofactor. On the left, the active zone protein complex containing RIM, RIM-BP, and Munc13 and a Ca^{2+} channel in the presynaptic plasma membrane is shown. In this protein complex, RIM binding to specific target proteins coordinates all three functions of the active zone: RIM binding to vesicular rab proteins (Rab3 and Rab27) mediates vesicle docking; and RIM binding to the central priming factor Munc13 activates vesicle priming; and RIM binding to the Ca^{2+} channel, both directly and indirectly via RIM-BP, recruits the Ca^{2+} channels within 100 nm of the docked vesicles for fast excitation-secretion coupling. The overall design of the neurotransmitter release

machinery depicted here enables in a single nanodevice fast and efficient triggering of release in response to action potentials by combing a fusion machine with a Ca^{2+} trigger and an active zone protein complex that positions all elements into appropriate proximity. Modified from Südhof, 2013 [10].

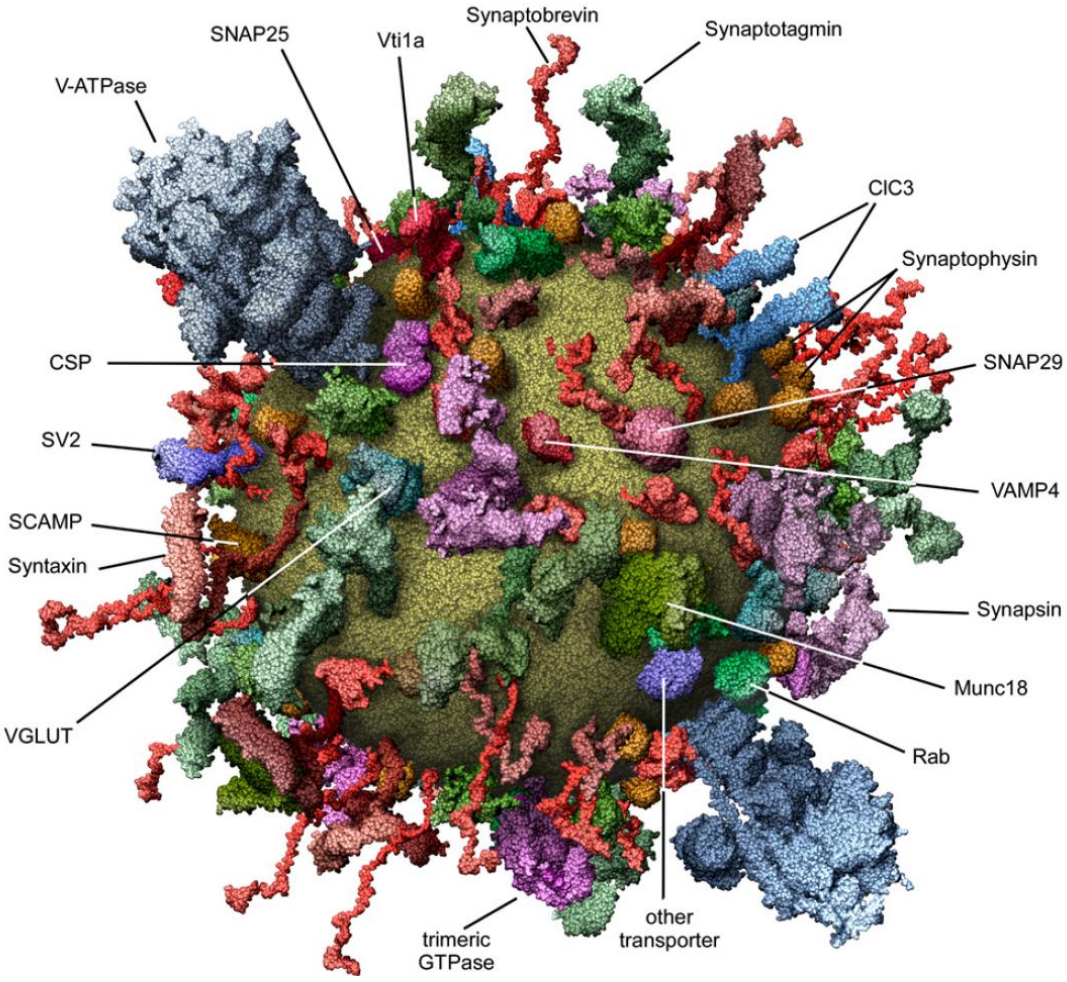

Figure 1-4 A molecular model of an average synaptic vesicle.

A scaled, schematic representation of an average synaptic vesicle based on the quantitative analysis of the major synaptic vesicle components including the lipids and proteins. The major synaptic vesicle residents are Synaptobrevin (~70 copies), Synaptophysin (~30-40 copies), Synaptotagmin (~15 copies), VGLUT (for a glutamatergic vesicle: ~10 copies) and the V-ATPase (~1-2 copies). The radius of a synaptic vesicle is ~20 nm. Taken from Takamori et al., 2006 [7].

The vesicle docking is followed by *vesicle priming*. The vesicle priming is a process where synaptic vesicle fusion machinery is primed into the energized form for setting the stage for fast Ca^{2+} triggering of neurotransmitter release. In this process, *SNARE* (*soluble NSF attachment protein receptor*) complexes are formed partially. SNARE complexes are composed of three SNARE proteins: *synaptobrevin 2* (also known as *VAMP-2*), which is indicated in Figure 1-3 and Figure 1-4, localized at synaptic vesicle membranes, *syntaxin-1* and *SNAP-25* localized at plasma membranes [10]. Before the complexes are formed, syantaxin-1 is transformed from a closed conformation into an open conformation by *Munc13* [10], as indicated in Figure 1-3 and Figure 1-4. In addition, *Munc18-1* binds to the synataxin-1 and regulates the formation of the SNARE complexes [10] as indicated in Figure 1-3 and Figure 1-4. In addition, *cysteine string proteins* (CSPs) as well as *synucleins* are known to modulate the SNARE complex assembly by direct binding to SNAP-25 or synaptobrevin 2, respectively [11,12].

After the vesicle priming, the vesicle fusion occurs. Upon SV fusion, SNARE complexes are fully assembled, which forces the fusing synaptic vesicle membranes and plasma membranes into close proximity. As a result, the SNARE complexes open fusion pores, which cause release of neurotransmitters from the vesicle lumen into the synaptic cleft. After the fusion, the SNARE complexes reside in the plasma membranes are disassembled by the action of *AAA+-ATPase NSFs* and its adaptors, *SNAPs* [13].

A final step of SV exocytosis is triggered by Ca^{2+}. Intracellular free Ca^{2+} concentration in a presynaptic terminal ($[Ca^{2+}]_{pre}$) is maintained as low as 0.05 – 0.1 μM mainly by the activity of the plasma membrane Ca^{2+}-ATPases (PMCAs) [14,15]. An opening of Ca^{2+} channels clustered at the active zones causes a rapid increase of $[Ca^{2+}]_{pre}$ to ~ 0.5 μM, and 10 APs at 100 Hz increased

$[Ca^{2+}]_{pre}$ further to ~2 μM [14].

Synaptotagmin 1 is a type I integral membrane protein preferentially expressed on SV membrane and exhibits low binding affinity to Ca^{2+} [16]. A large body of evidence has indicated that it is synaptotagmin 1 that synchronizes Ca^{2+} influx through the presynaptic Ca^{2+} channels to the rapid SV exocytosis. Although the mechanism of synaptotagmin 1 in Ca^{2+}-dependent SV exocytosis has not been completely understood, it has been proposed that its interaction with both SNAREs and acidic phospholipids is critically involved in this process.

Other than SNAREs and Synaptotagmin 1, multiple proteins including *complexin* and munc-18 are involved in Ca^{2+}-dependent SV exocytosis, and serve as regulatory elements in this series of molecular cascades (Figure 1-3) [10].

1.3.2 Endocytosis

Until recently, *clathrin-mediated endocytosis* (*CME*) (Figure 1-5) has long been thought to be a dominant endocytic pathway at synaptic boutons because previous work using clathrin-knockdown appeared to cause severe impairment of SV endocytosis [17]. The initial step of the CME pathway is formation of a *clathrin-coated pits* (*CCP*) with narrow necks at the synaptic membranes, which is followed by fission of this neck due to membrane scission mediated by *dynamin*, one of the GTPases [18]. After the fission, the vesicle sheds all the components of the coats.

In addition to the CME, other modes of endocytosis have also been proposed: *kiss-and-run* (*K&R*) endocytosis, *bulk endocytosis*, and *ultrafast endocytosis* (Figure 1-5). K & R is endocytosis likely coupled with exocytosis at the same site. An SV fuses with the plasma

membrane and is pinched off at the same location, while the SV retains its gross shape without undergoing full integration into the planar membrane [19].

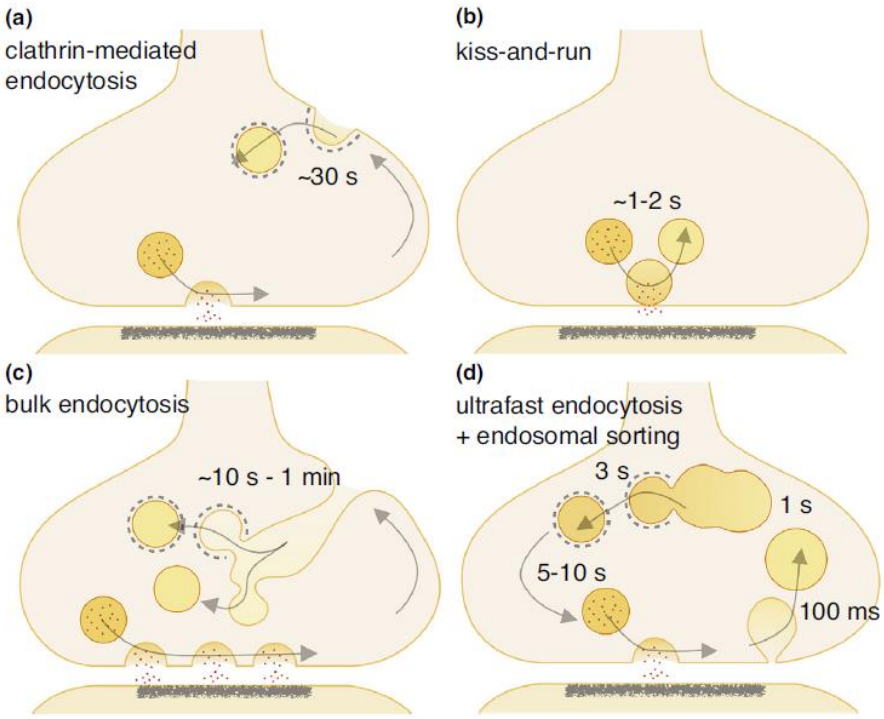

Figure 1-5 Four proposed modes of SV endocytosis at synapses.

(a) Full fusion of SVs followed by diffusion of SV constituents and endocytosis via CME at distal sites. **(b)** K & R: SV fusion pore opening and closing at the active zone which does not require full fusion of the SV membrane with the plasma membrane. **(c)** Intense stimulation-mediated fusion of multiple SVs followed by activity-dependent bulk endocytosis from distal sites. SVs may be reformed from cisternae using clathrin-dependent or clathrin-independent mechanisms. **(d)** Full fusion of SVs followed by ultrafast endocytosis and reformation of SVs by clathrin coats budding from endosomes. Note that time required for each mode of endocytosis substantially varies, ranging from ~100 ms for ultrafast endocytosis to ~1m min for bulk endocytosis. Taken from Watanabe et al., 2017 [20].

Bulk endocytosis occurs mainly during high neural activity [21], which is independent of clathrin [22]. Vacuoles retrieved by this endocytosis display large sizes (~80 -300 nm in diameter) [22-24], as compared to the size of a SV (~40 nm in diameter) [25]. Capacity of cargo selectivity of bulk endocytosis is poor compared to that of CME (Miller and Heuser, 1984; Nicholson-Fish et al., 2015). On the other hand, bulk endocytosis possesses high capacity to retrieve plasma membranes compared to CME [26-28]. Therefore, bulk endocytosis likely serves as an emergency endocytosis route for synapses to avert their surface expansion during periods of intense synaptic vesicle exocytosis.

Very recently, by combining optogenetic neural stimulation and a rapid freezing technique for sample processing for electron microscopy, ultrafast endocytosis that occurs at 200 times the speed of CME [29] has been proposed. Unlike CME, vesicles generated by this rapid endocytosis are not decorated by clathrin coats and their size is relatively larger than those generated by CME (~82 nm in diameter, ~2 fold larger than SVs) [29]. It is currently under intense debate which mode of endocytosis, CME or ultrafast endocytosis, is the predominant form of SV endocytosis at the presynaptic terminals.

1.3.3 Neurotransmitter uptake

Irrespective of the modes of endocytosis, newly regenerated SVs are empty and have to be reloaded with neurotransmitter molecules for the next round of exocytosis. Since classical neurotransmitters such as *glutamate, GABA, biogenic monoamines* and *acetylcholine* are locally generated or supplied at the presynaptic cytoplasm, SVs can be loaded with them immediately after their generation. Neurotransmitter transporters of synaptic vesicles (*vesicular*

neurotransmitter transporters; *VNTs*) are secondary transporters and, therefore, require a driving force generated by a concentration gradient of other ions. Unlike plasma membrane neurotransmitter transporters that utilize Na^+ concentration gradient across the plasma membrane, VNTs use a proton gradient across the SV membrane generated by the V-ATPases. Since proton has a positive charge, the entry of protons into SVs creates both a H^+ chemical gradient (ΔpH) and an electrical gradient (inside positive; also referred to as ΔΨ), a sum of which is called *a proton electrochemical gradient* ($\Delta\mu H^+$). Neurotransmitters are transported by using either ΔΨ, ΔpH or both depending on physical properties of neurotransmitters and the respective transporters (see also below).

So far, five distinct families of VNTs have been molecularly identified. Three *vesicular glutamate transporters* (*VGLUT1~3*) [30-36], one *vesicular GABA transporter* [37] which is also referred to as *vesicular inhibitory amino acid transporter*, *VIAAT* [38] (since it also transports glycine), two *vesicular monoamine transporters* (*VMAT1* and *VMAT2*) [39,40] which transport several biogenic amines such *dopamine*, *histamine*, *serotonin* with different affinities [41], *vesicular acetylcholine transporter* (*VAChT*) [42] and *vesicular nucleotide transporter* (*VNUT*) [43]. Consistent with their distant amino acid sequence homologies, these transporters utilize ΔpH and ΔΨ to different extents (Figure 1-6). Although the detail mechanisms are still under intense debate, it is currently proposed (mainly from biochemical experiments using native SVs or reconstituted transporters) that transport of negatively charged substances such as glutamate and nucleotide depends primarily on ΔΨ, whereas that of positively charged substances such as monoamines and ACh depends on ΔpH. Uptake of zwitter-ionic substances such as GABA depends equally on both gradients [44]. Therefore, alteration of the balance between ΔpH and ΔΨ has strong impact on the

rate of transport as well as the net amount of neurotransmitters accumulated into the SV lumen.

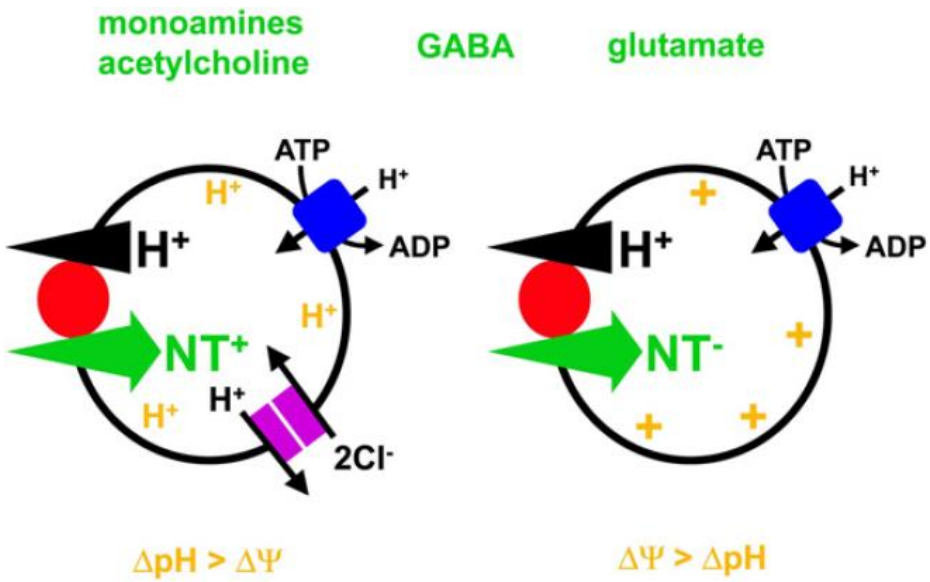

Figure 1-6 Vesicular neurotransmitter uptake.

The V-ATPase (blue) generates $\Delta\mu_{H+}$ that drives the accumulation of classical neurotransmitters (NT) into SVs. The movement of H^+ down their electrochemical gradient is coupled to the transport of transmitter in the opposite direction. Despite this common H^+ exchange mechanism, different vesicular neurotransmitter transporters (red) rely to differing extents on the two components of $\Delta\mu_{H+}$, the chemical gradient ΔpH and the electrical gradient Δψ. Vesicular monoamine and ACh transport, which involves the exchange of protonated cytosolic transmitter for two luminal H^+, involves more H^+ than charge movement and hence depends more on ΔpH than Δψ. On the other hand, transport of negatively charged glutamate depends more on Δψ than ΔpH. In the case of the zwitterion GABA, the transport equally depends on both ΔpH and Δψ. Intracellular chloride carriers such as ClCs (violoet) would promote vesicle acidification by dissipating the charge developed by the V-ATPase, secondarily activating the H^+ pump to make a larger ΔpH. Taken from Edwards, 2007 [44].

In addition to alteration of the $\Delta\mu H^+$, multiple factors, which can potentially affect quantal

size, have been proposed. First, alteration of cytosolic neurotransmitter concentrations may cause the alterations of quantal size. Biochemical assays using isolated SVs have indicated that higher the cytosolic concentrations of neurotransmitters are, more transmitters are transported into SVs with faster rates, although the transport system for neurotransmitters exhibits saturable nature [45,46]. This notion was substantiated by the fact that injection of exogenous glutamate into the presynaptic terminals of the calyx of Held synapses increased the amplitudes of excitatory postsynaptic currents [47-49]. Furthermore, expression of the vesicular transporters affects quantal sizes in multiple preparations. This was particularly supported by the experiments where VGLUTs were overexpressed either in rodent hippocampal neurons [50] or in neuromuscular junctions of drosophila lavae [51]. Since postsynaptic receptors are often not saturated by the amount of neurotransmitters released from a single synaptic vesicle, changes in quantal sizes by these mechanisms may have profound impact on the efficacy of neurotransmission.

1.4 Regulation of the $\Delta\mu_{H+}$

How is the balance between ΔpH and ΔΨ controlled? Since the V-ATPase is an electrogenic pump, entry of few protons already creates large ΔΨ, and this ΔΨ (inside positive) may repel the entry of further protons. Therefore, relatively large ΔΨ rather than ΔpH is built up in the absence of counter-ion movements. In turn, when counter-ions, such as inward movement of anions or outward movement of cations, were present, more protons could enter into SVs, thereby building up a larger ΔpH at the expense of ΔΨ (Figure 1-7). Thus, the balance between ΔpH and ΔΨ is regulated by the permeability of the SV membrane to various charged substances (e.g. ions) and their concentration gradients.

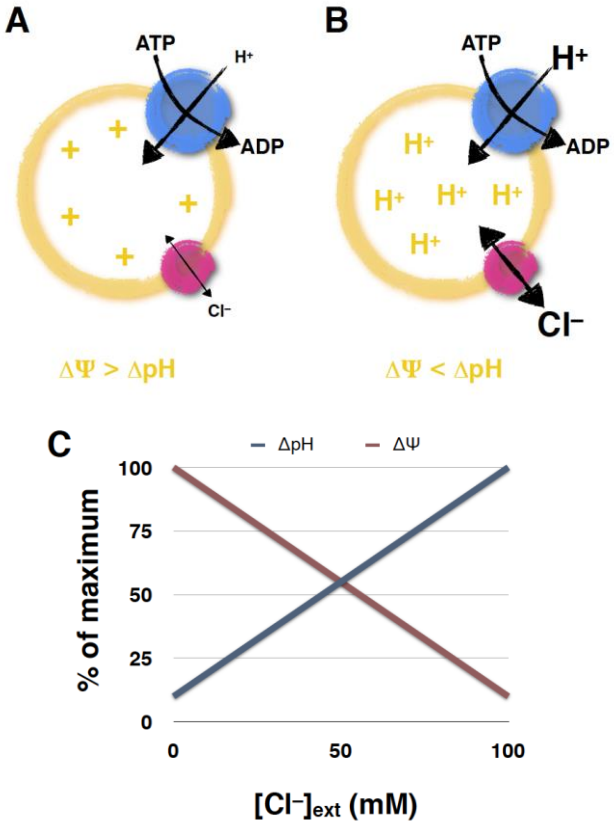

Figure 1-7 Electrogenic property of the V-ATPase.

V-ATPase (blue) utilizes an energy produced by ATP hydrolysis and generate proton gradient ($\Delta\mu H^+$) consisting of two components ($\Delta\psi$ and ΔpH). Since the V-ATPase is electrogenic, H^+ influx is critically restricted by $\Delta\psi$, and either accompanying anion influx or cation efflux is necessary to facilitate proton transport into the SV lumen. SV contain a putative Cl^- channel (pink; VGLUTs or ClC-3 may confer this activity). **(A)** In the presence of low Cl^- (or scant Cl^- permeability), H^+ influx is small and larger $\Delta\psi$ is generated. **(B)** In the presence of high Cl^-, Cl^- influx would dissipate $\Delta\psi$, and more H^+ can flow into SVs. As a result, largerΔpH is built up. **(C)** The relationship between $\Delta\psi$ and ΔpH as a function of external Cl^- concentrations. Both components can be monitored by fluorescent indicators such as acridine orange (for ΔpH) or oxonol (for$\Delta\psi$). Modified from Takamori, 2012 [52].

In fact, SVs contain various transporters or channels for ions that directly or indirectly modulate H^+ flux across SVs. For instance, it has been firmly demonstrated that SVs exhibit a Cl^- conductance that serves as a shunting current for H^+, resulting in an increase in net proton influx and thus a generation of larger ΔpH. CLC-type chloride channel family, ClC-3, was originally proposed as a prime candidate [53]. However, subsequent studies have demonstrated that, at least for glutamate-containing SVs, VGLUTs are responsible for Cl^--dependent facilitation of ΔpH. Importantly, the Cl^- conductance in VGLUTs has substantial impact on glutamate loading [54], although precise mechanisms of Cl^- action on glutamate transport is still elusive [55].

More recently, cation/H^+ exchange activity conferred by either Na^+/H^+ exchangers (NHEs) or VGLUTs (in the case of glutamate-containing vesicles) were shown to decrease ΔpH and consequently facilitate ΔΨ. Which isoform(s) of NHEs are involved, the cation specificities of the exchangers (Na^+ versus K^+), and their transport stoichiometry are currently under intense debate [56,57].

In stark contrast, the contribution of divalent cations such as Ca^{2+} and Zn^{2+} to the regulation of $\Delta\mu H^+$ has received less attention. To date, the mechanism and molecular entity of the transporting molecule(s) remain elusive. In the next chapter, I will explain current knowledge of the Ca^{2+} carriers on SVs, which is the main topic of this thesis work.

1.5 The candidates of Ca^{2+} transporters on SVs

Classical studies using SV fraction isolated from the electric organ of *Torpedo marmorata* revealed that SVs exhibited an ATP-dependent active Ca^{2+} transport activity [58-60]. Consistent with this, a transient increase of Ca^{2+} in the SV lumen was observed after stimulation at the cholinergic

synapse of the electric organ of Torpedo marmorata [61], suggesting that SVs can function as a Ca^{2+} store at presynaptic terminals in a physiological context.

Efforts to decipher the Ca^{2+}-transporting protein(s) in mammalian SVs have revealed, at least, two distinct activities. One is the vanadate-sensitive *P-type Calcium ATPases*, which were fully active at neutral pH, and whose activity was potently inhibited by vanadate (a broad inhibitor of P-type ATPases)[62]. In fact, two P-type ATPases, *plasma membrane Ca^{2+} ATPases* (*PMCAs*) and *sarcoplasmic endoplasmic reticulum Ca^{2+} ATPases* (*SERCAs*) have been identified in the SV proteome [7], although there are no evidence to demonstrate that these ATPases are generally functioning in native SVs. In addition to these primary ATPases well characterized in different organelles, purified SVs also exhibited a Ca^{2+}/H^{+} exchange activity conferred by a hitherto molecularly-unidentified protein optimally operational at pH 8.5 [62,63] (Figure 1-8). Not only characteristic responses to specific inhibitors, these two transport systems also exhibited substantial differences in their affinities for Ca^{2+}. While K_m of the vanadate-sensitive Ca^{2+} ATPase lies in the order of several hundred nM, K_m of the Ca^{2+}/H^{+} antiporter exceeds 300 μM, which far surpasses physiological calcium concentrations at presynaptic terminals [14]. Moreover, these transport systems exhibit characteristic dependence on Ca^{2+} concentrations. Notably, Ca^{2+} ATPase activity increases with Ca^{2+} concentration in the medium, reaching a maximum at ~25 μM, whereas its activity is inhibited at higher Ca^{2+} concentration and is completely abolished at ~500 μM Ca^{2+} [62].

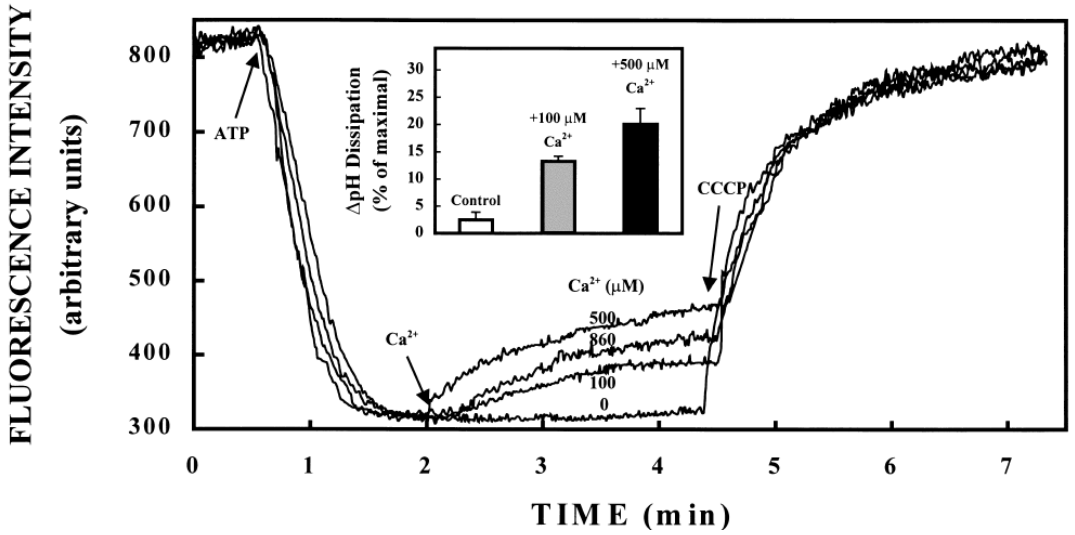

Figure 1-8 Effects of Ca^{2+} uptake on ΔpH of isolated SVs at pH 8.5.

The ΔpH of SVs isolated from sheep brain cortex was monitored using *acridine orange* (*AO*), a fluorescent ΔpH indicator. The decrease in AO fluorescence indicated acidification of the SV lumen. The reaction was started by adding ATP which activated V-ATPase, resulting in SV acidification monitored by quenching of AO fluorescence as described. At 2 min of the reaction, additions of Ca^{2+} reversed the AO fluorescence, extend of which depended on Ca^{2+} concentration, implying that H^+ efflux from SVs was induced upon Ca^{2+} entry. The protonophore CCCP (10 μM) was used to confirm that the pH gradient was formed by the V-ATPase. An inset represents the percentage of ΔpH reduction by Ca^{2+} relative to the control experiment in the absence of Ca^{2+}. Taken from Gonçalves et al., 1998 [63].

Aside from these two SV Ca^{2+} transport systems, it has been conjectured that one of the major SV proteins, SV2s (Synaptic Vesicle Glycoprotein 2s), may function as Ca^{2+} transporters in SVs [64]. SV2 was originally identified from the electric organ of Torpedo in 1985 [65], and the three different mammalian orthologs (SV2A, SV2B, and SV2C) were later identified [66-68]. According to their predicted structures with 12 transmembrane regions and their high

homologies with bacterial sugar transporters, transport functions have been proposed for SV2s. Interestingly, the genetic deletion of SV2 revealed synaptic phenotypes that could be well-explained by the increase in cytoplasmic [Ca^{2+}] [69,70] (Figure 1-9), leading to a plausible hypothesis that SVs may function as vesicular Ca^{2+} transporters. On the other hand, it was also reported that deletion of SV2A/SV2B produced decreased evoked synaptic responses without causing any changes in frequencies and amplitudes of the miniature excitatory synaptic currents (EPSCs), the size of readily releasable pool of vesicles, or the apparent Ca^{2+} sensitivity of vesicle fusion [71], which strongly argued against the hypothesis that SV2 functions as the Ca^{2+} transporter. Therefore, due to the lack of direct experimental proofs, the contribution of SV2s to the Ca^{2+} uptake into SVs has been enigmatic.

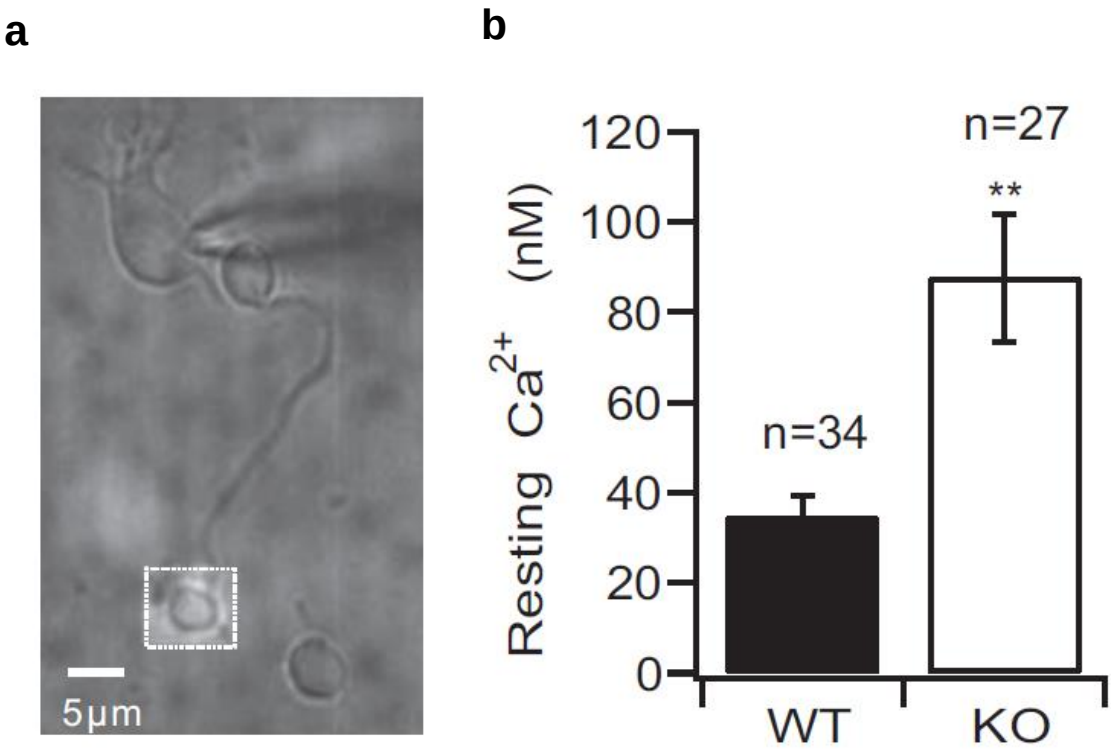

Figure 1-9 Absence of SV2B is associated with elevated resting presynaptic Ca^{2+}.
(a) An acutely isolated rod bipolar neuron is shown with a patch pipette on its soma. The dotted square over the terminal denotes the region from which the emitted bis-fura-2 fluorescence signal, which is a calcium indicator, was collected.
(b) The average resting Ca^{2+} concentration in synaptic terminals held at -70 mV is significantly higher in neurons from $SV2B^{-/-}$ mice (KO) than those from WT littermates. Error bars represent SEM. **p < 0.01. The internal Ca^{2+} concentration was determined from the ratio of fluorescence signals. Taken from Wan et al., 2010 [70].

1.6 The aim of this thesis work

A primary goal of this thesis work is to identify molecules responsible for Ca^{2+} transport into SVs, and to clarify uncertainties and controversial hypothesis related to the transport systems. To this end, I first set up experiments to reconcile the low affinity Ca^{2+}/H^{+} antiport activity, which was shown to be maximal at alkaline pH of 8.5 and exhibited low affinity for Ca^{2+}. Although the previous data was largely reproducible, I further found that the Ca^{2+}/H^{+} exchange activity exhibited much higher affinity than anticipated at neutral pH.

Second, I intended to identify which molecules, among the candidates for the vesicular Ca^{2+} transporter, were responsible for the high affinity Ca^{2+}/H^{+} antiport. For this purpose, specific inhibitors for the P-type ATPases, as well as SV fraction derived from SV2-deficient mice, were used. These experiments revealed that PMCAs, instead of SV2s or SERCAs, are the prime candidate for the vesicular Ca^{2+} transporter, which was responsible for both Ca^{2+} uptake as well as regulation of pH gradient across the SV membrane.

Finally, since the PMCAs have been characterized as plasma membrane residents, I

examined if PMCAs could reside also on SVs and possibly recycle within presynaptic terminals in vivo. For this purpose, a DNA construct encoding a PMCA1, one of the PMCA isoforms, in which a pH sensitive green fluorescent protein (SEP) was fused to the luminal portion, was transfected in cultured hippocampal neurons for live fluorescent imaging.

2. Material and Methods

2.1 Study approval

All experiments in this study were carried out under the approval of Doshisha University Animal Committee and Recombinant DNA Experiments Committee, and of the Institutional Animal Care and Use Committee of the RIKEN Kobe branch (approval number: QA2013-04-6). All experiments were performed in accordance with the guidelines and regulations of the respective institutions.

2.2 Animals

C57BL/6NJcl mice were purchased from CLEA or from Shimizu Laboratory Supplies, Japan. ICR mice were purchased from SLC, Japan. All mice were given food and water ad libitum. Animals were kept in an SPF facility with a 12-hour light and 12-hour dark cycle. The ambient temperature was maintained around 21˚C with a relative humidity of 50%. ICR mice (12 to 20 weeks old) were used as recipients. A combination anesthetic (0.75 mg/kg of medetomidine, 4.0 mg/kg of midazolam, and 5.0 mg/kg of butorphanol) was used for surgery. The anesthetics were administered to recipient mice by intraperitoneal injection. All animal experiments were approved by the Institutional Animal Care and Use Committee of the RIKEN Kobe branch (approval number: QA2013-04-6) and the Institutional Animal Care and Use Committee of Doshisha University.

2.3 One-cell embryo microinjection

C57BL/6N females (4–6 weeks old) were superovulated and mated with C57BL/6N males. Fertilized eggs were collected from the ampulla of the oviduct of plugged C57BL/6N females by micro-dissection and kept in KSOM medium (Merck Millipore) in a 5% CO_2 incubator at 37 ˚C. *Cas9* mRNA (100 ng/μL) and six gRNAs (50 ng/μL each, 300 ng/μL total) were co-injected into the cytoplasm of fertilized eggs in M2 medium (Merck Millipore) at room temperature. Details of the cytoplasmic injection procedure have been described previously [72]. After microinjection, the injected embryos were cultured for 1 hr in KSOM medium (Merck Millipore) in a 5% CO_2 incubator at 37˚C, then 15–30 embryos were transferred to the oviducts of recipient ICR female mice.

2.4 One-step generation of double gene knockouts of SV2A/2B and SV2B/2C

Double gene knockout (DKO) mice of SV2A/2B and SV2B/2C were generated by the triple-target CRISPR method [73]. Briefly, *Cas9* mRNA and sgRNAs were synthesized according to the protocol reported previously [73]. All gRNAs were selected from pre-made design in Database (http://crispr.riken.jp). *Cas9* mRNA (100 ng/μL) and six gRNAs (50 ng/μL each, 300 ng/μL total) were injected into the cytoplasm of fertilized eggs of C57BL/6NJcl mice. For SV2A/2B DKO, six gRNA targets were used (Sv2a_8 5’-AAGGCGAACGCATGGCAGAT-3’, Sv2a_9 5’-GCGTAAAGATCGGGAAGAAT-3’, Sv2a_25 5’-GGCAGCCTTCCTTATTGTGC-3’, Sv2b_28 5’-CTGGCAATCGAAGGGCAATC-3’, Sv2b_38 5’-GTGGACCCTCTTCTTCGTCT-3’, Sv2b_41 5’-AGGTATCGGGACAACTATGA-3’). For SV2B/2C DKO, six gRNA targets were used (Sv2b_28, Sv2b_38, Sv2b_41, Sv2c_56 5’-ACTGGAATGGAATACGAGAA-3’, Sv2c_77

5’-AGACCTATGCATACCAAATT-3’, Sv2c_78 5’-CACAAACACCTCCACGCCAT-3’).

2.5 Synaptic vesicle isolation

Crude synaptic vesicle fraction (LP2) was isolated from mouse whole brain with slight modifications [74]. Briefly, whole brains from C57BL/6 (B6N) mice were homogenized in homogenization buffer (320 mM sucrose, 4 mM $MgSO_4$, 4 mM HEPES-NaOH, pH 7.3), and applied a series of centrifugation steps as indicated in Figure 2-1. The final membrane pellet (LP2) was resuspended in standard acidification buffer (300 mM sucrose, 4 mM $MgSO_4$, 10 or 20 mM MOPS-KOH, pH 7.2), and stored at –80˚C until use. Essentially, all fluorometric assays, unless indicated otherwise, were performed with this fraction. For determination of apparent affinity of Ca^{2+}/H^+ exchange activity and radioactive $^{45}Ca^{2+}$ uptake, LP2 obtained from Wistar rat or B6N mouse brains was further purified as indicated in Figure 2-1. The further purified pellet (SV) was resuspended in acidification buffer and stored at –80˚C until use.

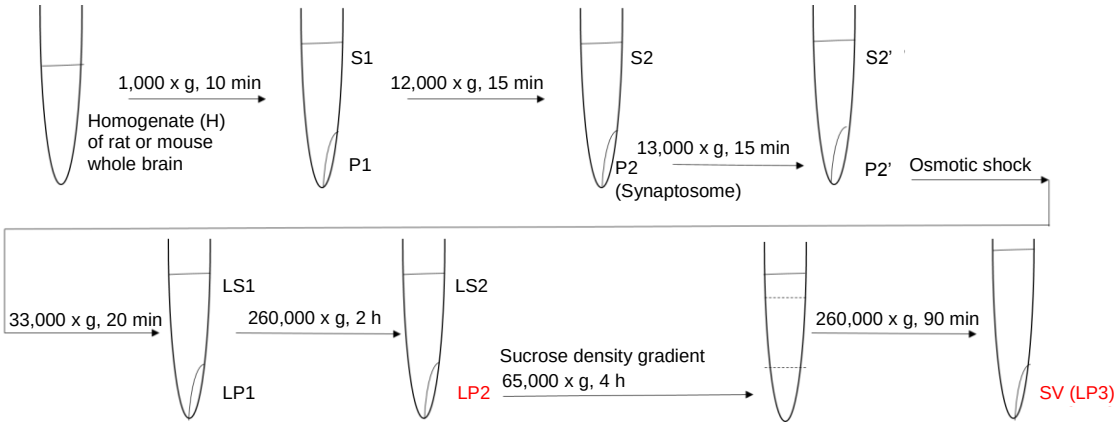

Figure 2-1 Purification of SVs from rat or mouse brains.

A flow diagram of purification of SVs from rat or mouse brains. The homogenate was centrifuged for 10 min at 1,000 x *g*, and the resulting supernatant (S1) was centrifuged for 15 min at 12,000 x *g*. The resulting pellet (P2) was washed with homogenization buffer and re-centrifuged for 15 min at 13,000 x *g* to obtain crude synaptosomes (P2'). To release SVs from the synaptosomes, P2' fraction was subjected to an osmotic shock by the addition of 9 volume of ice-cold water and the subsequent homogenization. The resulting suspension was centrifuged for 20 min at 33,000 x *g*. After the centrifugation, the supernatant (LS1; lysate supernatant) was centrifuged for 2 hours at 260,000 x *g*. The final membrane pellet (LP2) was resuspended in standard acidification buffer. In addition, as necessary LP2 was further purified by sucrose gradient centrifugation (50 – 800 mM continuous gradient). After centrifugation at 65,000 × g_{max} for 4 hours, turbid materials visible in the middle of the gradient (in the range of 200 to 400 mM sucrose) were pooled and sedimented by centrifugation at 260,000 × g_{max} for 90 min (SV fraction). The resulting pellet (SV) was resuspended in acidification buffer.

2.6 Measurement of vesicle acidification with acridine orange

Acidification measurements were performed according to previous publications using acridine orange (AO, Molecular Probes), which is permeant weak base dye, as a ΔpH reporter [54]. The pKa (~10) of this probe is higher compared to the optimum pKa (5 – 8) for reporting acidification of SVs, which cause poor signal noise ratio due to high background. On the other hand, AO provides adequate signal in response to acidification of SVs.

When AO is diluted in aqueous solutions, it is mainly monomeric, whereas upon increase in concentration will form dimers, trimers or higher order oligomers. The equilibrium between monomeric and dimeric/oligomeric AO is also affected by pH of its surrounding environment. While at neutral pH monomeric AO (mAO) is the dominating form, a decrease in pH shifts the

equilibrium towards dimers/oligomers [75]. Therefore, when AO is in the lumen of an organelle which acidifies, aggregated AO will be formed in the lumen, which cannot permeate the bilayer membranes unlike monomers. This leads to an increase in the population of aggregated AO, and in turn a decrease in the number of monomers [76] as indicated in Figure 2-2a. Since these forms of AO have distinct excitation and emission maxima, the acidification process can be monitored by measuring the optical response of either of these forms as indicated in Figure 2-2b. In conventional bulk acidification assays, emission [77] or absorbance [57,78] of mAO is monitored.

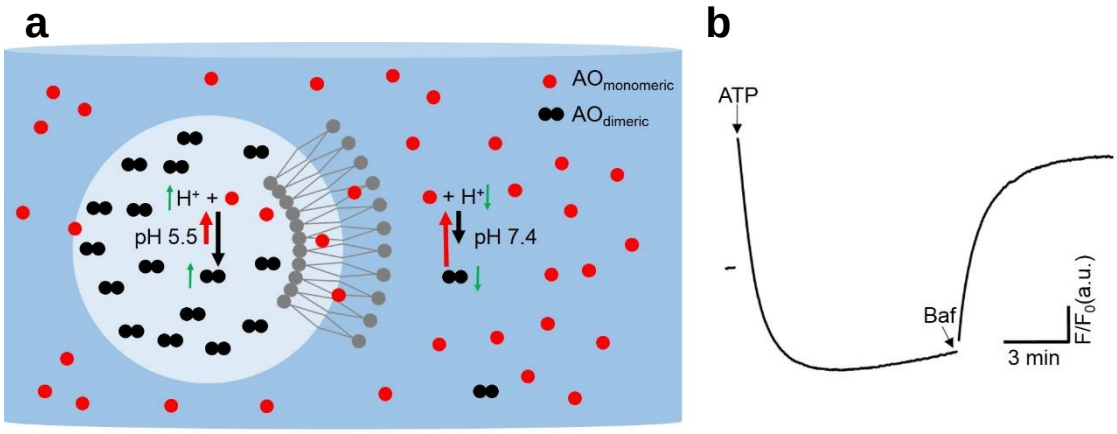

Figure 2-2 The characteristics of acridine orange and its response to acidification.
(a) Schematic representation of the proposed mechanism by which AO reports acidification of the lumen of SVs. As depicted, $AO_{monomeric}$ (red circle) is membrane-permeable and highly abundant at alkaline pH of 7.4. On the other hand, $AO_{dimeric}$ (black double circles), which is the dominant form of AO at low luminal pH of 5.5 cannot, cannt pass the lipid bilayer of the SVs and is trapped in the acidified lumen. Upon acidification of SVs, the number of $AO_{monomeric}$ molecules in the solution decreases while the number of $AO_{dimeric}$ in the vesicular lumen will increase.
(b) A typical trace of acidification assay with 20 µg LP2 with 1.5 µM AO in MOPS-based assay buffer containing 100 mM KCl. Addition of 2 mM ATP dramatically decreased AO

fluorescence, indicating that the lumens of SVs were acidified. Subsequent addition of 500 nM *bafilomycin A_1* (*Baf*) recovered the fluorescence signal indicating alkalization of the vesicular lumen.

In my research, changes in AO fluorescence (excitation at 492 nm and emission at 530 nm with slit length of 2.5 nm, HMT 700V) was monitored in a Hitachi F2500 fluorometer (Hitachi, Japan) at 32˚C, unless otherwise stated [54]. Typically, 20 µg of LP2 or SV fraction was preincubated in 1 ml of assay buffer (300 mM sucrose, 4 mM $MgSO_4$, 1.5 µM AO, 10 or 20 mM MOPS, pH 7.2) with varying composition of 5 mM K-glutamate, 3 mM or 100 mM KCl, 50 µM EGTA, and 50 µM BAPTA as indicated in the figures or figure legends. After a stable baseline was achieved (usually within 10 min), 2 mM ATP was added to start acidification. Various concentrations of $CaCl_2$ or 50 µM other divalent cations were added 10 min after the start of the acidification. At the end of recordings, a V-ATPase inhibitor, bafilomycin A_1 (500 nM) was added to ensure that quenching of AO was due to proton translocation by the V-ATPase. In experiments in Figure 3-6, 3-8, and 3-9, 15 µM cyclopiazonic acid, 500 µM vanadate, or 30 µM levetiracetam was pre-incubated for 10 min before measurements. Representative traces from multiple measurements are shown in the figures. For estimation of temperature co-efficient (Q_{10}) for the Ca^{2+}-dependent AO de-quenching, acidification assays were performed at two different temperatures. The Q_{10} was calculated from an equation:

$$Q_{10}=\left(\frac{\tau_1}{\tau_2}\right)^{\wedge}\left(\frac{10}{T_2-T_1}\right),$$

in which τ_1 and τ_2 are time constants of recovery rates of acridine orange fluorescence after the addition of Ca^{2+} at temperature T_1 and T_2. T_1 and τ_2 were obtained by a first order exponential fitting using a Solver function in Excel software. T_1 and T_2 ($T_2 > T_1$) are 32.3 and 37.3 ˚C, respectively.

2.7 Calculation of free calcium concentrations

Free calcium concentration was calculated by solving simultaneous equations in four unknowns: concentration of Ca^{2+} binding with BAPTA ([CaBAPTA]), that of Mg^{2+} binding with BAPTA ([MgBAPTA]), that of Mg^{2+} binding with ATP ([MgATP]) and that of Ca^{2+} binding with ATP ([CaATP]) as follows.

$$K'_{\mathrm{CaBAPTA}}=\frac{[\mathrm{CaBAPTA}]}{([Ca^{2+}]_T-[\mathrm{CaBAPTA}]-[\mathrm{CaATP}])([\mathrm{BAPTA}]_T-[\mathrm{CaBAPTA}]-[\mathrm{MgBAPTA}])}$$

$$K'_{\mathrm{MgBAPTA}}=\frac{[\mathrm{MgBAPTA}]}{([Mg^{2+}]_T-[\mathrm{MgBAPTA}]-[\mathrm{MgATP}])([\mathrm{BAPTA}]_T-[\mathrm{CaBAPTA}]-[\mathrm{MgBAPTA}])}$$

$$K'_{\mathrm{CaATP}}=\frac{[\mathrm{CaATP}]}{([Ca^{2+}]_T-[\mathrm{CaBAPTA}]-[\mathrm{CaATP}])([\mathrm{ATP}]_T-[\mathrm{CaATP}]-[\mathrm{MgATP}])}$$

$$K'_{\mathrm{MgATP}}=\frac{[\mathrm{MgATP}]}{([Mg^{2+}]_T-[\mathrm{MgBAPTA}]-[\mathrm{MgATP}])([\mathrm{ATP}]_T-[\mathrm{CaATP}]-[\mathrm{MgATP}])}$$

$[Ca^{2+}]_T$, $[Mg^{2+}]_T$, $[BAPTA]_T$ and $[ATP]_T$ are the total concentrations of each substance. $[Ca^{2+}]_T$ is calculated from an equation $[Ca^{2+}]_T = [Ca^{2+}]_{add} + [Ca^{2+}]_{ctm}$, where $[Ca^{2+}]_{add}$ and $[Ca^{2+}]_{ctm}$ are concentrations of added $CaCl_2$ and of contaminated Ca^{2+} determined routinely by fura-2 assay,

respectively. $K'_{CaBAPTA}$, $K'_{MgBAPTA}$, K'_{CaATP} and K'_{MgATP} are the overall apparent association constants. Microsoft Excel Solver was used to solve the equations.

To set up the equations above, the overall apparent association constants, K's ($K'_{CaBAPTA}$, $K'_{MgBAPTA}$, K'_{MgATP} and K'_{CaATP}) were converted from the absolute association constants, Ks, which were determined for standard conditions (see details in Appendixes and in Marks and Maxfield [79]). Table 5-1 lists the published association constants for BAPTA and ATP, as well as the ΔH values for BAPTA and ATP. ΔH values were necessary for the conversions from the absolute association constants to the overall apparent association constants (see details in Appendixes).

2.8 Measurement of Ca^{2+} uptake

The concentrations of SV or LP2 fractions were adjusted to 0.2 mg/mL in sucrose buffer. 100 µL aliquots were preincubated for 10 min at 32°C. The reaction was started by addition of 10 µM (final concentration) $^{45}Ca^{2+}$ dissolved in sucrose buffer containing ATP (2 mM), vanadate (500 µM), EosinY (10 µM), cyclopiazonic acid (15 µM) and levetiracetam (30 µM) when indicated. All incubations contained 0.125% (v/v) DMSO and 0.167% (v/v) ethanol in a final volume of 150 µL. After incubation for 10 min at 32°C, the reaction was stopped by addition of 3 mL of ice-cold buffer, followed by filtration through nitrocellulose filters. The incubation tubes were washed out with 3 mL of ice-cold buffer, and the wash out buffer was poured through the filter. The filters were washed out twice with 2.5 mL of ice-cold buffer. Radioactivities retained on filters were measured by liquid scintillation counting using an ALOKA LSC-6100 liquid scintillation counter (ALOKA, Japan).

2.9 Western blot analysis

SDS-PAGE was used to separate 20 µg of LP2 fractions from wild-type or SV2-DKO mice. Proteins were transferred to a PVDF membrane. The resulting blots were probed with isoform specific antibodies for SV2s (Synaptic Systems, Germany) or with a pan-SV2 monoclonal antibody (a kind gift from Reinhard Jahn, Göttingen, Germany). For detection, the appropriate secondary antibodies conjugated to horseradish peroxidase were used. After washing steps, the horseradish peroxidase was detected by enhanced chemiluminescence using a commercially available kit (Perkin Elmer, Inc., MA). As loading controls, anti-synaptophysin monoclonal antibody (Cl7.2, Synaptic Systems, Germany) was used.

2.10 Molecular cloning of PMCA1−SEP, Syntaxin-1a-SEP and SypHy

To construct PMCA1-SEP, a full length mouse PMCA1 (accession no. NM_001359506.1) was amplified by PCR from mouse adult brain cDNA generated using SuperScript RT-PCR system (Invitrogen) and subcloned into a *Stu*I site of pCR-Blunt vector (Thermo Fisher Scientific). A DNA fragment encoding the N-terminal region of PMCA1 (a.a. 1-139) with linker sequence (STSGGSGGTGGS) and a fragment of super-ecliptic pHluorin (SEP) amplified from SypHy plasmid [17,80] (a kind gift from Leon Lagnado) were amplified by PCR and cloned into an *Eco*RV site of pcDNA3.1(+) using In-Fusion Cloning Kit (Clontech). A DNA fragment encoding the C-terminal region of PMCA1 (a.a. 140-1,220) was PCR-amplified and cloned into a *Not*I site of pcDNA3.1(+) which contained the N-terminal region of PMCA1 and SEP using In-Fusion Cloning Kit. To construct Syntaxin1a-SEP, a full length mouse Syntaxin-1a (accession no.

NM_016801.3) without the stop codon and a fragment of SEP were amplified by PCR and simultaneously cloned into a *Nhe*I/*Eco*RV site of pcDNA3.1(+). A DNA fragment encoding SypHy [17] was amplified by PCR and subcloned into a *Nhe*I/*Xba*I site of pcDNA3.1(+).

2.11 Neuronal cultures

Primary hippocampal cultures were prepared from embryonic day 16 ICR mice as described previously [81] with slight modifications. Briefly, hippocampi were dissected and were incubated with papain (90 units/mL, Worthington) for 20 min at 37˚C. After digestion, hippocampal cells were plated onto poly-D-lysine-coated coverslips in 24- or 12-well plates (Falcon) at a density of 20,000 cells/cm^2 and kept in a 5% CO_2 humidified incubator. At 2-4 days *in vitro* (DIV), 40 μM FUDR (Sigma) and 100 μM uridine (Sigma) were added to inhibit the growth of glial cells. One-fifth of the culture medium was replaced with fresh medium every 2-4 days. Cultures were transfected with plasmids encoding either PMCA1-SEP, SypHy, or Syntaxin-1a-SEP at 5-7 DIV using CalPhos™ mammalian transfection kit (Clontech) in accordance with a calcium phosphate transfection method which is optimized for neuronal cultures [82], and were subjected to experiments at 12-14 DIV. Animals for the primary neuron cultures were treated according to our institutional guidelines for the care and use of animals (Doshisha University).

2.12 Immunostaining

At DIV12, neural cells were fixed with 4% (wt/vol) paraformaldehyde in phosphate buffer (Wako) for 10 min at room temperature (RT). After washing with phosphate buffered saline (PBS), the neurons were permeabilized with PBS containing 0.1% Triton X-100 for 20 min at RT, and

incubated with PBS containing 10% (vol/vol) fetal bovine serum (FBS) and 0.1% Triton X-100 for 30 min at RT. The cells were incubated with rabbit polyclonal anti-GFP antiserum (1:1,000) and mouse monoclonal anti-Synaptophysin antibody (1:1,000; C17.2) (both were kind gifts from Reinhard Jahn) for 1 hour at RT. The cells were rinsed three times with PBS, and further incubated with Alexa-488-conjugated anti-rabbit IgG (1:1,500; Invitrogen) and Alexa-555-conjugated anti-mouse IgG (1:1,500; Invitrogen) for 30 min at RT. After washing steps, Alexa-488 or Alexa-555 fluorescence was acquired with 470/22 nm excitation and 514/30 nm emission filters or 556-to 570-nm excitation and 600- to 650-nm emission filters, respectively.

2.13 Live imaging of SEP

To examine the localization and the recycling behavior of PMCAs in living neurons, I took an advantage of a pH-sensitive green fluorescent protein variant, super-ecliptic pHluorin (SEP) with an apparent pKa of ~ 7.1. When the SEP molecule is fused to a luminal region of synaptic vesicle protein, such as synaptobrevin 2 (VAMP2), it is quenched (dim) due to the acidic vesicular pH (Figure 2-3a). When SVs fuse with the plasma membrane, the SEP molecule is exposed to an extracellular solution at pH 7.4, thereby increasing its fluorescence. In this way, the SEP imaging allows us to monitor the recycling behavior of proteins of interest tagged with SEP. In addition, by measuring SEP fluorescence intensities upon sequential application of an acidic solution and a NH_4Cl solution, vesicular pH in which the SEP probe is located as well as the surface fraction of the SEP probe can be estimated (Figure 2-3b).

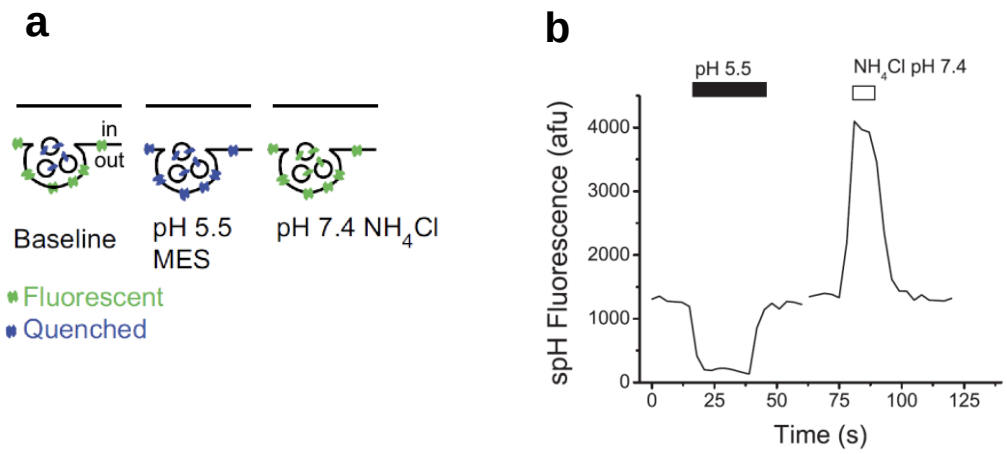

Figure 2-3 The synapto-pHluorin (spH) assay.

The spH is a fusion protein in which a variant of pH-sensitive green fluorescent protein (ecliptic pHluorin: SEP) is fused to the luminal domain of synaptobrevin2 (VAMP2). Exposure to pH 5.5 quenches the spH fluorescence on the axon surface, and application of NH_4Cl raises the intra-vesicular pH to ~7.4, thereby dequenching vesicular the spH fluorescence, as shown graphically in **(a)**. **(b)** A representative trace of the spH fluorescence at presynaptic terminal upon exposure to buffer containing 25 mM MES at pH 5.5 and 50 mM NH_4Cl at pH 7.4. Modified from Mani and Ryan, 2009 [83].

Cells cultured on a glass coverslip were placed in a custom-made imaging chamber on a movable stage and continuously perfused with standard extracellular solution containing (in mM): 140 NaCl, 2.4 KCl, 10 HEPES, 10 glucose, 2 $CaCl_2$, 1 $MgCl_2$, 0.02 CNQX, and 0.025 D-APV (pH 7.4). A solution containing 50 mM NH_4Cl (pH 7.4) was applied directly onto the area of interest with a combination of a fast flow exchange microperfusion device and a bulb controller, both of which were controlled by Clampex 10.2. To estimate luminal pH and surface fraction of the SEP probes, a MES-buffered solution at pH 5.5 and 50 mM NH_4Cl (pH 7.4) were successively

applied to cultured neurons as described previously [81]. Briefly, SEP fluorescence during acid quenching (F_Q) and during subsequent NH_4Cl application (F_{NH4Cl}) was measured. The observed fluorescence in a given terminals is thought to be the sum of the fluorescence derived from the surface fraction of the probes (S) that experiences extracellular pH and from the vesicular fraction (1 – S) that is exposed to luminal pH (pHv). The fluorescence during the baseline (F_0) and the fluorescence during F_Q are expressed as

$$F_0 = S \times F_{pH\ 7.4} + (1 - S) \times F_{pHv} \quad \ldots(i),$$

$$F_Q = S \times F_{pH\ 5.5} + (1 - S) \times F_{pHv} \quad \ldots(ii),$$

where $F_{pH\ 5.5}$ and F_{pHv} are the total fluorescence values predicted when all probe molecules in a terminal are exposed to pH 5.5 and pH_v, respectively. By solving Equations (i) and (ii), S and $F_{pHv} / F_{pH\ 7.4}$ were calculated as follows:

$$S = (F_0 / F_{pH\ 7.4} - F_Q / F_{pH\ 7.4}) / (1 - F_{pH\ 5.5} / F_{pH\ 7.4}),$$

$$F_{pHv} / F_{pH\ 7.4} = (F_0 / F_{pH\ 7.4} - S) / (1 - S).$$

According to the Henderson-Hasselbalch equation, $F_{pH\ 5.5} / F_{pH\ 7.4}$ was given as follows:

$$F_{pH\ 5.5} / F_{pH\ 7.4} = (1 / (1 + 10^{pKa - 5.5})) / (1 / (1 + 10^{pKa - 7.4})),$$

where the pK_a value of SEP estimated previously by using SypHy was 7.1 [84].

Finally, SV pH (pH_v) was then calculated as follows:

$$pH_v = pK_a - \log((1 + 10^{pK_a - 7.4}) / F_{pHv} / F_{pH\ 7.4} - 1).$$

Fluorescence imaging was carried out at room temperature (~27ºC) on an inverted microscope (Olympus) equipped with a 60× (1.35 NA) oil immersion objective and 75 W Xenon lamp. Images (1024 × 1024 pixels) were acquired with a scientific cMOS camera (ORCA-Flash 4.0, Hamamatsu Photonics) with 100 ms exposure time under the control of MetaMorph software (Molecular Devices). Fluorescence of SypHy, PMCA1-SEP or Syntaxin-1a-SEP was imaged with 470/22 nm excitation and 514/30 nm emission filters.

For live imaging, images were acquired in time-lapse mode at 1 Hz under control of MetaMorph software. Field stimulation was delivered via bipolar platinum electrodes with 1 msec constant voltage pulses (50 V). A solution containing 50 mM NH_4Cl was applied at the end of recordings as described above.

3. Results

3.1 A Ca^{2+}/H^{+} exchanger in SVs operates at neutral pH

Evidence that SVs isolated from sheep brain cortex contain low affinity Ca^{2+}/H^{+} antiport activity relied essentially on an acidification assay in which fluorescence quenching of acridine orange due to V-ATPase-dependent acidification was reversed by addition of Ca^{2+} [62,85,86]. This activity was characterized by its low affinity (Km > 200 μM) and operated at pH 8.5. However, chelation of Ca^{2+} by EGTA would result in rapid liberation of H^{+} from EGTA, and the ability of Ca^{2+} chelation by EGTA depends critically on pH. As such, addition of Ca^{2+} in the presence of EGTA during the measurement may have caused a change in pH, raising the possibility that the affinity and pH dependence may have been disturbed. Therefore, I decided to use BAPTA whose K_D is similar to that of EGTA, but the ability to chelate Ca^{2+} is much less affected by pH changes. First, I tested the effect of Ca^{2+} in the presence of BAPTA at neutral pH of 7.2, and compared with that in the presence of EGTA (Figure 3-1a). Acidification of crude SV fraction (LP2) was induced by adding 2 mM ATP in the presence of 100 mM Cl^{-}, and 600 μM Ca^{2+} was then added. As observed in previous studies at pH 8.5 [85,86], slow alkalization of SVs was also observed in the presence of EGTA (Figure 3-1a, red trace in the left panel). Notably, the effect of Ca^{2+} was more pronounced when the assay was performed in the presence of BAPTA (Figure 3-1a, red trace in the right panel). I should point out that the binding rate constant of BAPTA is higher than that of EGTA. In addition, the calcium chelation of EGTA may cause some potential errors in the acidification assay, because EGTA releases H^{+} upon the chelation of Ca^{2+} at neutral pH (i.e. pH 7.2), because the nitrogens of EGTA bind protons with *pKa*s of 8.96 and 9.58[87]. Moreover, it is

possible that Ca^{2+} chelation of the EGTA is inhibited by the binding of Mg^{2+} in the assay buffer more strongly with EGTA than with BAPTA. Figure 3-1a also indicates that the Ca^{2+}/H^{+} exchange activity was also operative at neutral pH. Essentially, the same results were obtained under conditions where acidification was monitored in SVs pre-acidified by VGLUT-mediated glutamate transport [54] (Figure 3-1 b), confirming that the activity originated from SVs rather than contaminating organelles such as microsomes and mitochondria. To further confirm if the de-quenching represented a transporter-mediated process, I measured de-quenching velocities upon the addition of Ca^{2+} at various temperatures (32.3 ˚C and 37.3 ˚C) under the same conditions as those in Figure 3-1b (right panel). The temperature co-efficient (Q_{10}) was estimated to be ~ 1.6 (Figure 3-1c), which is within the range of physical properties of transporter-mediated processes rather than simple diffusion [88,89].

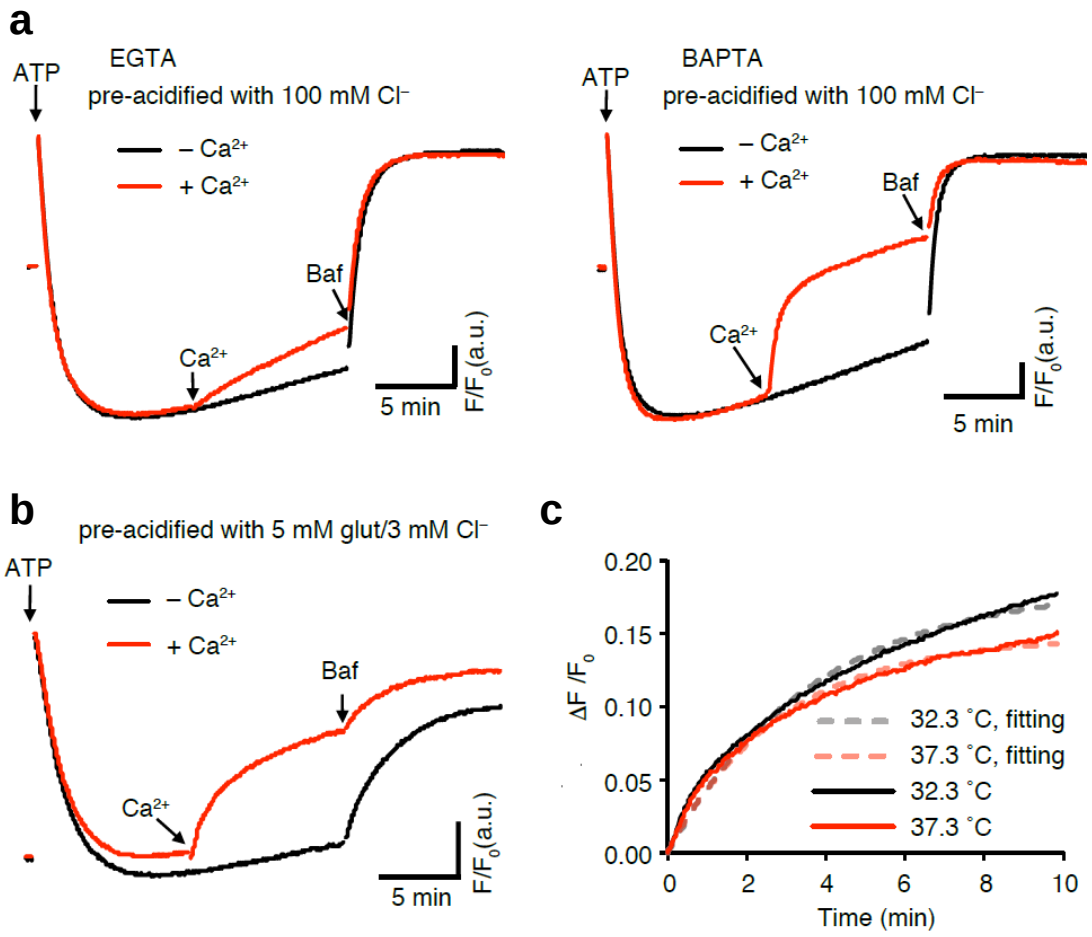

Figure 3-1 Ca^{2+}/H^{+} exchange activity attenuates ΔpH in synaptic vesicles at neutral pH.

(a) Effect of Ca^{2+} in the presence of EGTA (left) or BAPTA (right) on ATP-dependent acidification at pH 7.2. Acidification was measured using acridine orange as a reporter dye. Crude SV fraction (LP2) was incubated in the presence of 50 µM EGTA or 50 µM BAPTA in the presence of 100 mM KCl. To initiate acidification, 2 mM ATP was added, and 600 µM $CaCl_2$ (only for red traces) and 500 nM bafilomycin (Baf) were added at time points indicated by arrows. Note that de-quenching (indicated by increases in fluorescence) upon the addition of $CaCl_2$ was greater in the presence of BAPTA than EGTA. The traces were the representative traces from more than three measurements.

(b) Effect of Ca^{2+} in the presence of BAPTA on ATP-dependent, glutamate-induced acidification at pH 7.2. Crude SV fraction (LP2) was incubated in the presence of 50 µM BAPTA in the presence of 5 mM glutamate and 3 mM KCl. To initiate acidification, 2 mM ATP was added, and 600 µM $CaCl_2$ (only for red traces) and 500 nM bafilomycin (Baf) were added

at time points indicated by arrows. The traces were the representative traces from more than three measurements.

(c) Temperature coefficient (Q_{10}) of Ca^{2+}-induced alkalization. Ca^{2+}-induced alkalization of SVs that were pre-acidified in the presence of 5mM glutamate and 3mM KCl was monitored either at 32.5˚C (black) or at 37.5˚C (red). The alkalization kinetics were obtained by exponential fittings shown in dotted lines. Q_{10} was calculated as described in Materials and Methods.

3.2 The vesicular Ca^{2+}/H^+ exchanger exhibits high affinity to Ca^{2+}

To estimate the affinity of the Ca^{2+}/H^+ exchanger in SVs at neutral pH, I measured alkalization of pre-acidified SVs by various concentrations of $CaCl_2$ in the presence of a fixed concentration of BAPTA (50 µM). To this end, I first estimated free Ca^{2+} concentrations in my assay buffers using fura-2 as a Ca^{2+} indicator and found it to be ~ 1 µM (Figure 3-2).

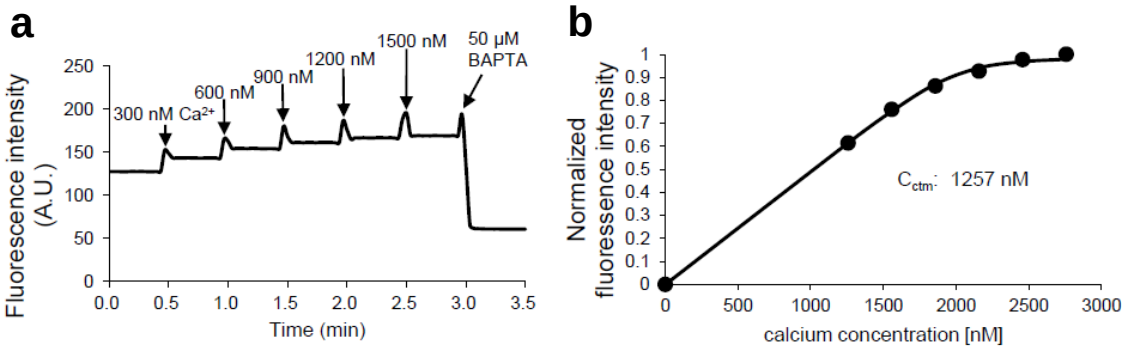

Figure 3-2 Contaminated Ca^{2+} in experimental solutions was determined using a fura-2 assay.

(a) Fluorescence intensity of fura-2 in a cuvette with various concentrations of Ca^{2+}. 1 ml of assay buffer (100 mM KCl, 10 mM MOPS-KOH, pH7.2) was preincubated for 10 min. The preincubation was followed by adding 300, 600, 900, 1200 and 1500 nM of total exogenous

$CaCl_2$. Finally, 50 μM BAPTA was added at the time points indicated by the arrows.

(b) Fluorescence intensity (FI) above the intensity of fluorescence with 50 μM BAPTA was plotted against the added Ca^{2+} concentrations. FI was normalized by maximum FI obtained at 1500 nM exogenous Ca^{2+}. The data points were fitted with the following equation (see detail in Iino [90]):

$$FI = \left[C_T + C_f + K_d - \left\{\left(C_T + C_f + K_d\right)^2 - 4C_T C_f\right\}^{1/2}\right] / \left(2C_f\right),$$

where $C_T = C_{add} + C_{ctm}$

C_T, C_{add}, C_{ctm}, C_f and K_d are concentrations of total Ca^{2+} including contaminated Ca^{2+}, of exogenously added Ca^{2+}, of contaminated Ca^{2+} in assay buffer, of added fura-2, and the dissociation constant of Ca·fura-2, respectively. Microsoft Excel Solver was used to solve the equations.

As a result, the C_{ctm} was 1257 nM.

In addition, the C_{ctm} of the assay buffer without KCl was estimated in the same procedure. The C_{ctm} in this situation was 875±9.32 (s.e.m., n = 3) nM. Moreover, the C_{ctm} of ultra pure water (MilliQ) was estimated. The C_{ctm} in this situation was 740±41.3 (s.e.m., n = 4) nM. Taking the above results of the C_{ctm} into consideration, I regarded C_{ctm} as 1 μM in the calculation of free Ca^{2+} concentration in Figure 3-3.

Taking this into account, free Ca^{2+} concentrations in the assay buffer were set by adding $CaCl_2$ (see Materials and Methods for details). After complete acidification of SVs in the presence of 100 mM KCl was achieved, I added a series of Ca^{2+} concentrations ranging from 0 to 75 μM that were equivalent to 3.63 to 6410 nM free [Ca^{2+}] in the assay medium. With the ranges of Ca^{2+} added, the rate of alkalization increased as a function of free Ca^{2+} concentrations (Figure 3-3a). A plot of initial velocities of alkalization as a function of free Ca^{2+} concentrations revealed that K_m

of Ca^{2+}-induced SV alkalization was ~ 400 nM (Figure 3-3b), a value that appeared to be several magnitudes lower than that reported previously [85].

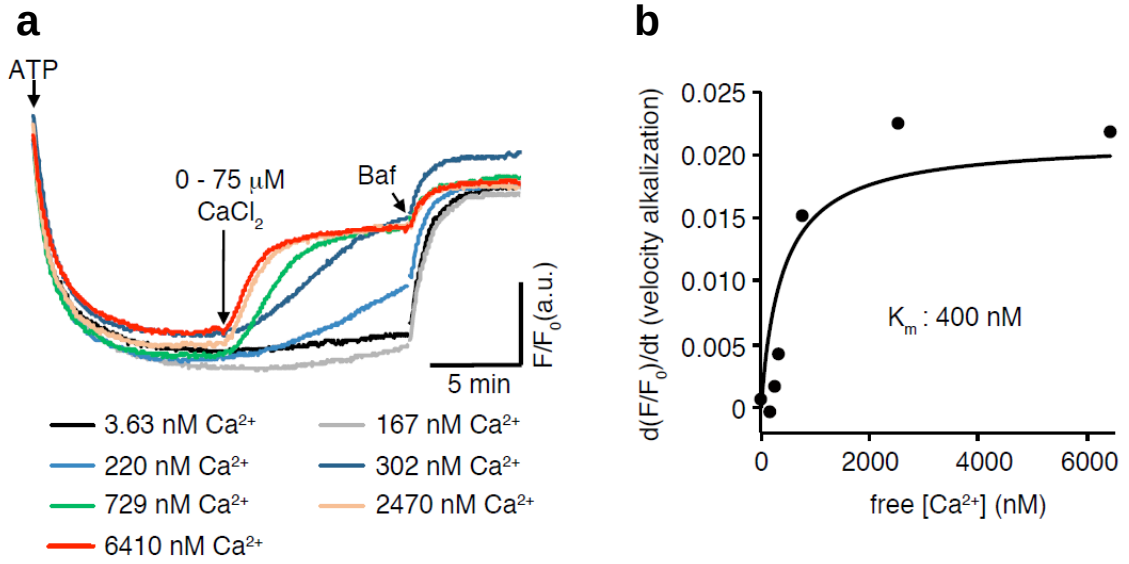

Figure 3-3 Apparent affinity of the Ca^{2+}/H^+ exchanger on SVs.

(a) Alkalization of SVs by various concentrations of Ca^{2+}. After SVs were maximally acidified in the presence of 100 mM KCl, various concentrations of $CaCl_2$ were added. Individual traces in the presence of various free [Ca^{2+}], ranging from 3.63 – 6410 nM of free [Ca^{2+}] were color-coded.

(b) The initial slopes of alkalization in (a) were plotted against free [Ca^{2+}]. Data points were fitted with the Michaelis-Menten equation to calculate K_m.

To further characterize the Ca^{2+}/H^+ antiport activity at neutral pH, I tested a series of divalent cations for the ability to alkalize pre-acidified SVs. Previous studies demonstrated that, at alkaline pH, Zn^{2+} and Cd^{2+} are substrates of the same Ca^{2+}/H^+ exchanger, whilst Ba^{2+} and Sr^{2+} are not [91].

In my assay conditions in the presence of BAPTA at pH 7.2, $Zn^{2+}$and Cd^{2+} induced alkalization of pre-acidified SVs in the presence of 100 mM KCl to a similar extent as that of Ca^{2+}, whereas Ba^{2+} induced slower but significant alkalization (Figure 3-4).

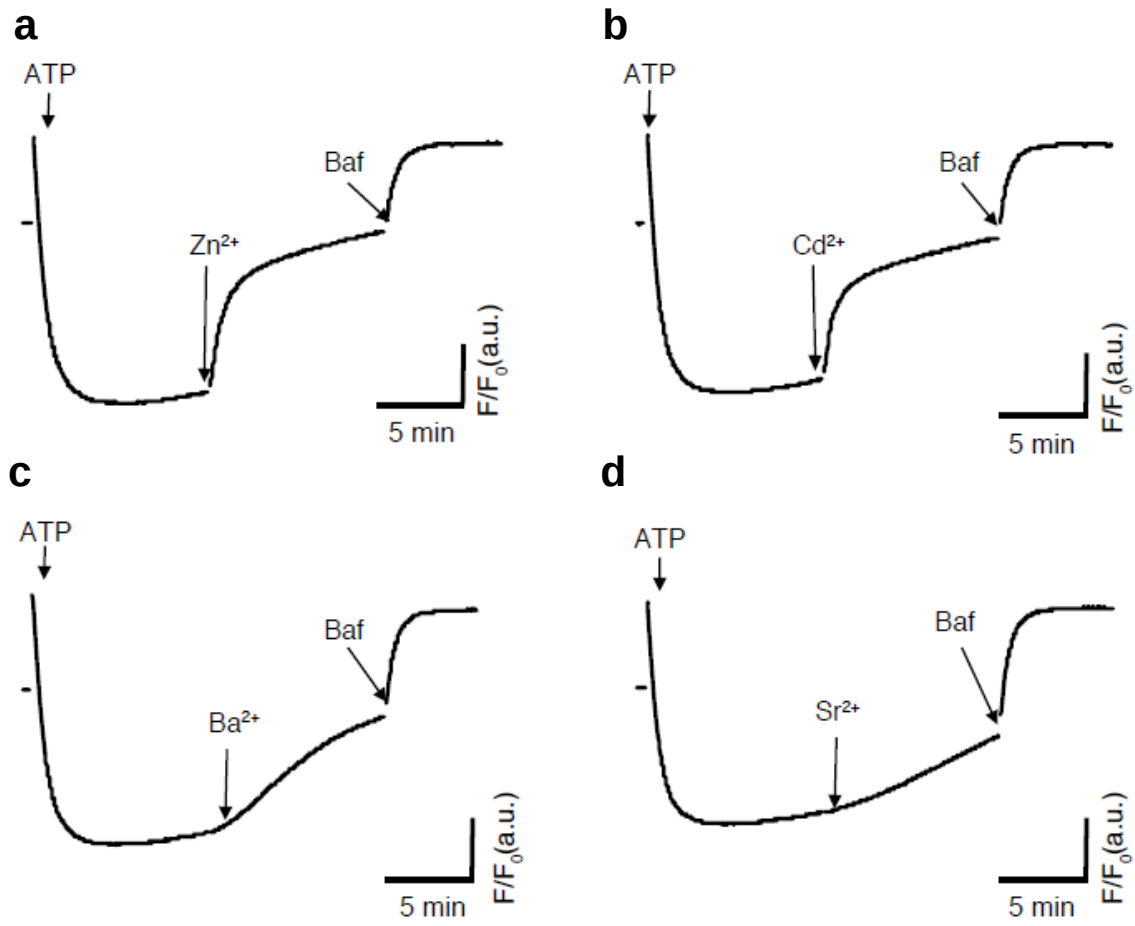

Figure 3-4 Selectivity of the Ca^{2+}/H^{+} exchanger for other divalent cations.

LP2 fraction was acidified in the presence of 100 mM KCl at pH 7.2. After stable baselines were achieved, various divalent cations including Zn^{2+}, Cd^{2+}, Ba^{2+}, and Sr^{2+} at final concentration of 50 µM were added. The traces were the representative traces from more than three measurements. Note that I observed the same results when vesicles were pre-acidified in the presence of 5 mM glutamate and 3 mM KCl (see Figure 3-5).

Consistent with previous results, Sr^{2+} showed marginal alkalization, indicating that the Ca^{2+}/H^{+} exchanger in SVs shows substrate preference as follows: $Ca^{2+} \approx Zn^{2+} \approx Cd^{2+} > Ba^{2+} \gg Sr^{2+}$. The same trend was observed when LP2 was pre-acidified by glutamate, indicating that the alkalization by divalent cations originated from VGLUT-containing SVs (Figure 3-5). It should be noted here that it remains unknown if these divalent cations are transported by distinct transporters with similar proton coupling, or if the alkalization resulted from the blockade of the V-ATPase activity.

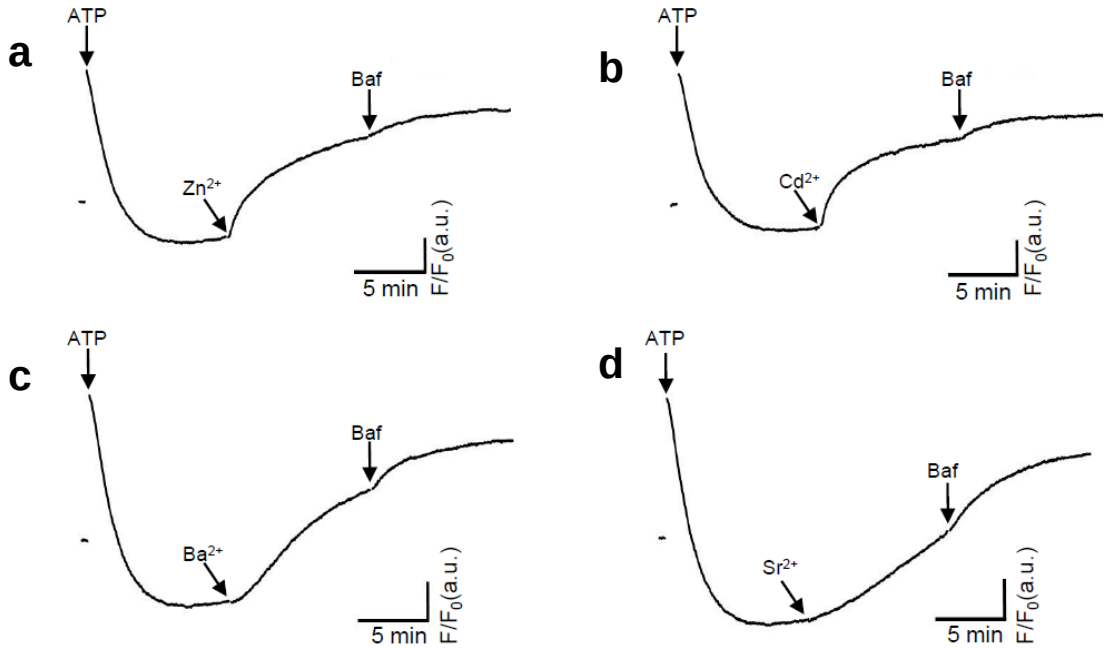

Figure 3-5 Selectivity of the Ca^{2+}/H^{+} exchanger of VGLUT-containing SVs for other divalent cations.

LP2 fraction was acidified in the presence of 5 mM glutamate and 3 mM KCl at pH 7.2. After stable baselines were achieved, various divalent cations including Zn^{2+} **(a)**, Cd^{2+} **(b)**, Ba^{2+} **(c)**, and Sr^{2+} **(d)** at final concentration of 50 µM were added.

3.3 SV2s are not responsible for Ca^{2+}/H^{+} exchange in SVs

As described in the Introduction, there are several candidates responsible for Ca^{2+} transport in SVs. Comprehensive proteomic analysis of purified SV fraction identified two P-type ATPases, PMCA and one that exchanges Ca^{2+} from the cytosol with protons in the lumen of sarcoplasmic endoplasmic reticulum (SERCA) [7]. However, contributions of these ATPases to SV acidity due to a H^{+} coupling have not been directly investigated. Furthermore, according to synaptic phenotypes related to changes in presynaptic Ca^{2+} concentrations and in presynaptic calcium buffering in SV2-deficient neurons [69,70], it has been hypothesized that SV2s may be involved in Ca^{2+} transport into SVs. I therefore sought to clarify which protein was responsible for the observed Ca^{2+}/H^{+} exchange activity in SVs at neutral pH.

First, in order to verify the contribution of SV2s in Ca^{2+}/H^{+} exchange, I generated SV2A/2B- and SV2B/2C-double knockout (DKO) mice using the CRISPR/Cas9 system. I then tested if Ca^{2+}/H^{+} exchange activity was affected. Western blot analysis of LP2 fractions purified from SV2A/2B-DKO or SV2B/2C-DKO mice using isoform-specific antibodies confirmed efficient gene knockout by the CRISPR/Cas9 system (Figure 3-6a). Moreover, western blot analysis using a pan-SV2 antibody that equally recognizes all SV2 isoforms revealed that SV2A and SV2B represented the major SV2 isoforms in brain, and expression of SV2C was minor (Figure 3-6a). As a control, I confirmed that expression of synaptophysin, an abundant SV protein [7], was unaltered in SVs derived from SV2-deficient mice. As shown in Figure 3-6b, Ca^{2+}/H^{+} exchange activity was normal in SVs from SV2A/2B-DKO mice, and the extent of alkalization induced by 50 μM $CaCl_2$ was comparable to that observed in SVs from wild-type mice of the same age (Figure 3-6b).

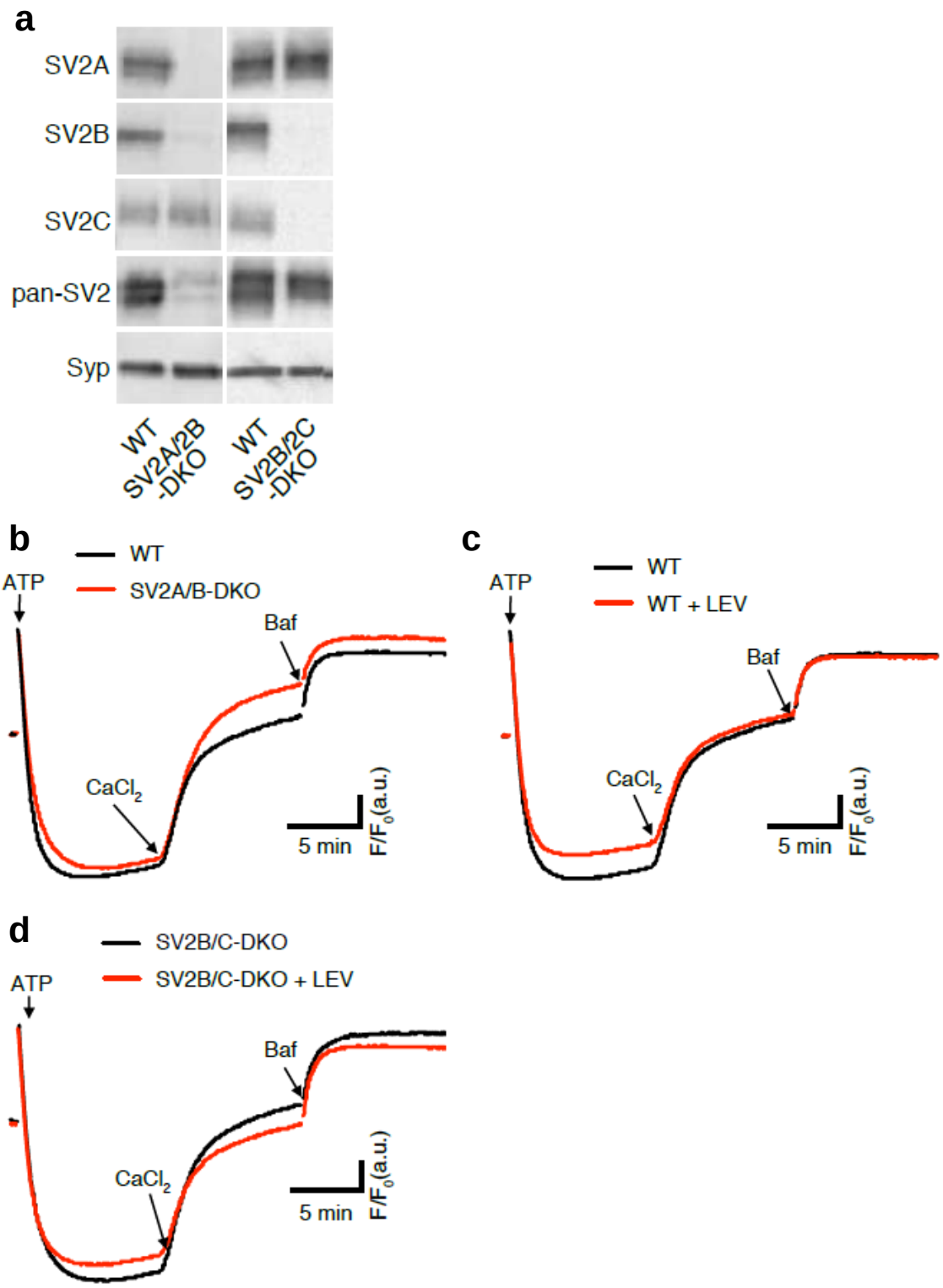
a
SV2A
SV2B
SV2C
pan-SV2
Syp
WT
SV2A/2B -DKO
WT
SV2B/2C -DKO
b
WT
SV2A/B-DKO
ATP
Baf
CaCl2
5 min
F/F0(a.u.)
c
WT
WT + LEV
ATP
Baf
CaCl2
5 min
F/F0(a.u.)
d
SV2B/C-DKO
SV2B/C-DKO + LEV
ATP
Baf
CaCl2
5 min
F/F0(a.u.)

Figure 3-6 SV2s do not confer Ca^{2+}/H^{+} exchange.

(a) Expression of SV2 isoforms in synaptic vesicles derived from SV2A/B-DKO and SV2B/C-DKO mice. Equal amounts of vesicle proteins from each genotype (20 µg/lane) were analyzed by western blotting using isoform-specific antibodies. Antibodies used for western blots are indicated at the left of the images. Rabbit polyclonal antibodies against SV2A, SV2B, and SV2C, and a mouse monoclonal antibody that recognizes all SV2 isoforms (pan-SV2) were used. For loading controls, a mouse monoclonal antibody against synaptophysin (Syp) (Cl7.2) was used. Note that expression of the SV2 isoforms was completely abolished in the respective DKO samples. A faint band revealed by the pan-SV2 antibody in the SV2A/2B-DKO sample indicated that SV2C content was much less than that of SV2A or SV2B. The images were cropped from four independent blots for presentation, and the original digital images of the full-length blots are presented in Figure 3-7.

(b) Ca^{2+}-induced alkalization in vesicles derived from SV2A/B-DKO (red) compared to wild-type mice (black). 50 µM $CaCl_2$ was added after vesicles were pre-acidified in the presence of 100 mM KCl.

(c) Effect of levetiracetam (LEV, 30 µM) on Ca^{2+}-induced alkalization in vesicles from wild-type mice. Vesicles were pre-acidified in the presence of 100 mM KCl, and 50 µM $CaCl_2$ was then added. LEV pre-treatment (red traces) shows little impact on alkalization by Ca^{2+} compared to the respective controls without LEV pre-treatment (black traces).

(d) Effect of levetiracetam (LEV, 30 µM) on Ca^{2+}-induced alkalization in vesicles from SV2B/2C-DKO mice. Measurements were performed as in (c). LEV pre-treatment (red traces) shows little impact on alkalization by Ca^{2+} compared to the respective controls without LEV pre-treatment (black traces).

Traces in (b) – (d) are the representative data from two to three measurements in each condition.

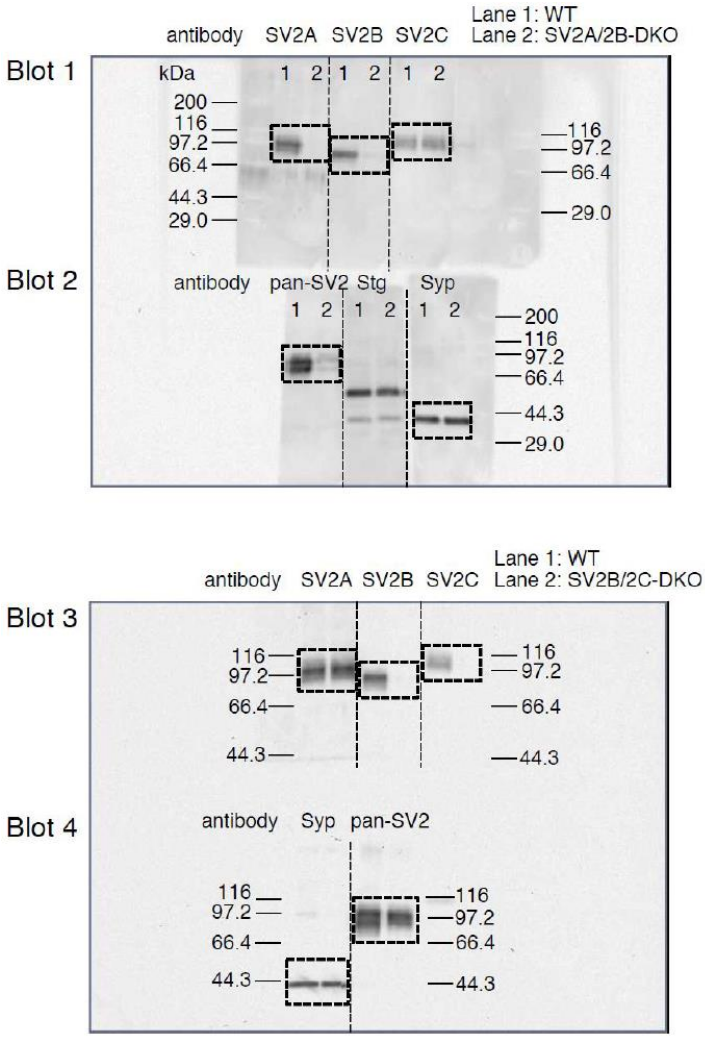

Figure 3-7 The raw data of the western blotting of Figure 3-6a.

Upper panel shows two original blots to produce the left panel of Fig. 4a. The blots were cut into pieces that contained protein samples from wild-type and SV2A/2B-DKO brains. The blot with antibody against Synaptotagmin 1 (Stg) was not used for the main figure. The areas used for the main figures are indicated by botted squares. Molecular weight standards (Protein Molecular Weight Marker (Broad), Takara Bio Inc., Japan) are indicated at the side of the blots. Bottom pannel shows two original blots to produce the right panel of Fig. 4a. The blots were cut into pieces that contained protein samples from wild-type and SV2B/2C-DKO mice.

Antibodies used were indicated at the top of the blots. Rabbit polyclonal antibodies against SV2A, SV2B, and SV2C were purchased from Synaptic Systems (see https://www.sysy.com/

and references therein). A mouse monoclonal antibody against synaptophysin (Syp) [92] and a monoclonal antibody that recognizes all SV2 isoforms (pan-SV2) [65] were kind gifts from Reinhard Jahn (Göttingen, Germany).

Levetiracetam (LEV, also known as Keppra® or E Keppra®) is an established second-generation antiepileptic drug, whose molecular target is SV2A [93]. LEV selectively binds to the cytoplasmic portion of SV2A [93,94] and potentially inhibits SV2A function [94]. The inability of LEV to inhibit Ca^{2+}/H^{+} exchange (Figure 3-6c) in SVs from wild-type mice provided further support that SV2A was not responsible for the activity, although SV2B, another isoform of SV2s, was present in the SV preparation. To completely rule out the contribution of SV2A to Ca^{2+}/H^{+} exchange activity, I examined the effect of LEV on transport activity in SV2B/2C-DKO samples (note that only SV2A is present in SV2B/2C-DKO mice). Again, LEV did not reduce Ca^{2+}-induced alkalization (Figure 3-6d). Taken together, although SV2s have been proposed to function as Ca^{2+} transporters in SVs, SV2s do not contribute to high affinity Ca^{2+}/H^{+} exchange activity at neutral pH.

3.4 The plasma membrane Ca^{2+} ATPases (PMCAs) mediate Ca^{2+}/H^{+} exchange in SVs.

Next, I examined the effect of blockers that selectively inhibit the P-type Ca^{2+} ATPases, including PMCAs and SERCA. Among the available inhibitors, 500 μM vanadate, a PMCA blocker, potently inhibited Ca^{2+}-induced alkalization of SVs (Figure 3-8a). On the other hand, 15 μM cyclopiazonic acid (CPA), a SERCA inhibitor [95], did not affect alkalization by Ca^{2+} (Figure 3-8b), indicating that the high affinity Ca^{2+}/H^{+} exchange activity observed with this assay was

attributed to PMCAs.

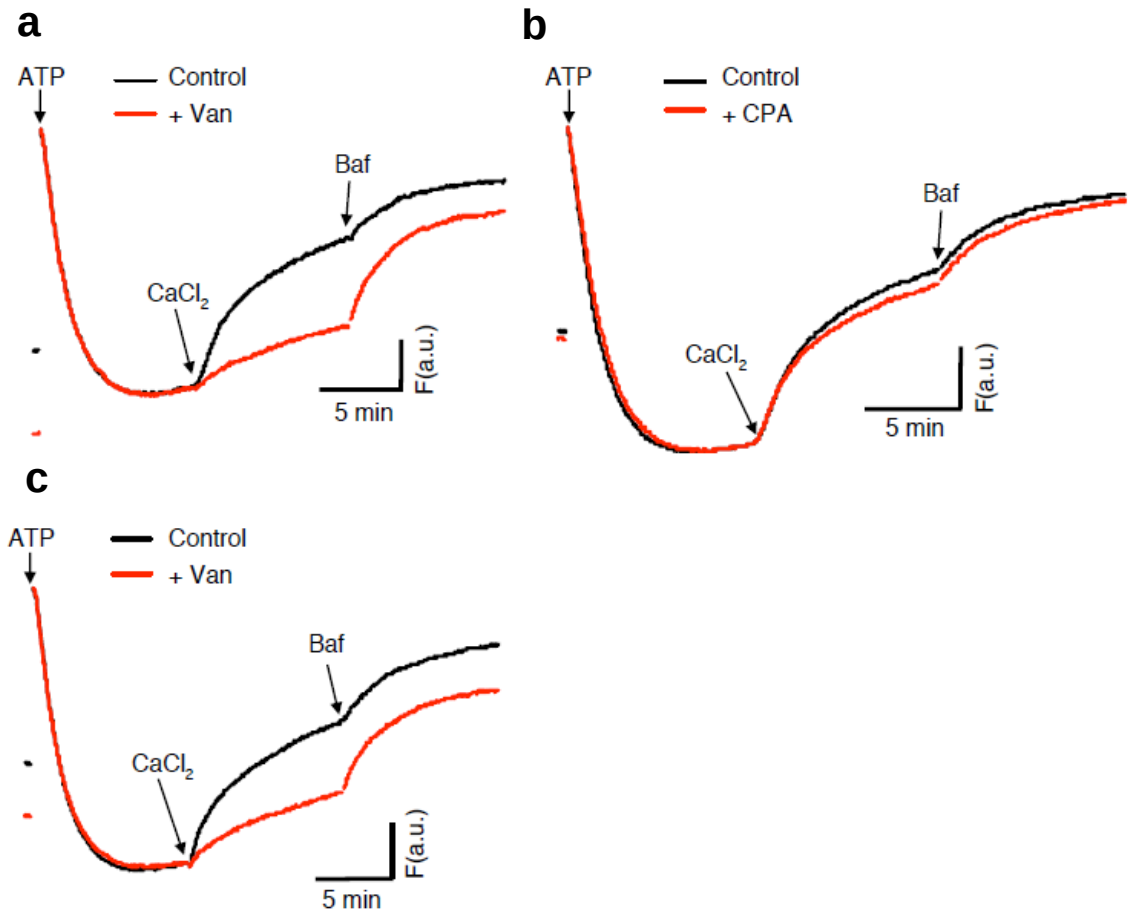

Figure 3-8 PMCAs predominantly contribute to Ca^{2+}/H^{+} exchange.

(a) Effect of vanadate (Van, 500 µM) on Ca^{2+}-induced alkalization. Vesicles were pre-acidified in the presence of 5 mM glutamate and 3 mM KCl in the absence (black) and presence (red) of 500 µM Van, and 50 µM $CaCl_2$ was added to induce alkalization. In these experiments, pure SV fractions were used to exclude possible contributions of other membrane contaminants.

(b) Effect of CPA (CPA, 15 µM) on Ca^{2+}-induced alkalization. Vesicles were pre-acidified in the presence of 5 mM glutamate and 3 mM KCl in the absence (black) and presence (red) of 15 µM CPA, and 50 µM $CaCl_2$ was added to induce alkalization.

(c) Effect of Van (500 µM) on Ca^{2+}-induced alkalization by 500 µM $CaCl_2$. Measurements

were performed as in (a) except that a high concentration of $CaCl_2$ (500 μM) was added. All traces are the representative data from at least two to three measurements in each condition. Since vanadate slightly reduced AO quenching signals in the presence of 5 mM glutamate and 3 mM KCl, fluorescence traces were normalized by amplitudes of acidification, and the starting points of alkalization by $CaCl_2$ were adjusted for comparison.

Notably, whereas Ba^{2+}- and Sr^{2+}-induced alkalization of pre-acidified SVs by glutamate was largely abolished in the presence of vanadate, alkalization induced by Zn^{2+} or Cd^{2+} was not completely blocked by vanadate (Figure 3-9). These observations implied that, while Ba^{2+} and Sr^{2+} are recognized by PMCAs, there are other divalent cation/H^+ exchangers that transfer Zn^{2+} or Cd^{2+}. Of note, ZnT-3, a vesicular Zn^{2+} transporter, is present on a subpopulation of SVs that contain glutamate [96-98], and therefore could contribute to vanadate-insensitive Zn^{2+}/H^+ exchange activity observed here, although the precise mechanism of Zn^{2+} transport into SVs, e.g. proton coupling during transport cycles, remains to be determined.

It was previously reported that in sheep SVs, vanadate-sensitive Ca^{2+} transport activity was largely absent in the presence of > 200 μM Ca^{2+} [62]. However, Ca^{2+}-induced alkalization at neutral pH was evident by 500 μM Ca^{2+} under my assay conditions (Figure 3-8c, black trace). More importantly, 500 μM vanadate effectively impeded the alkalization (Figure 3-8c, red trace), indicating that even in the presence of higher concentrations of Ca^{2+}, Ca^{2+}-induced alkalization was mediated by PMCAs, irrespective of the Ca^{2+} concentrations within this range.

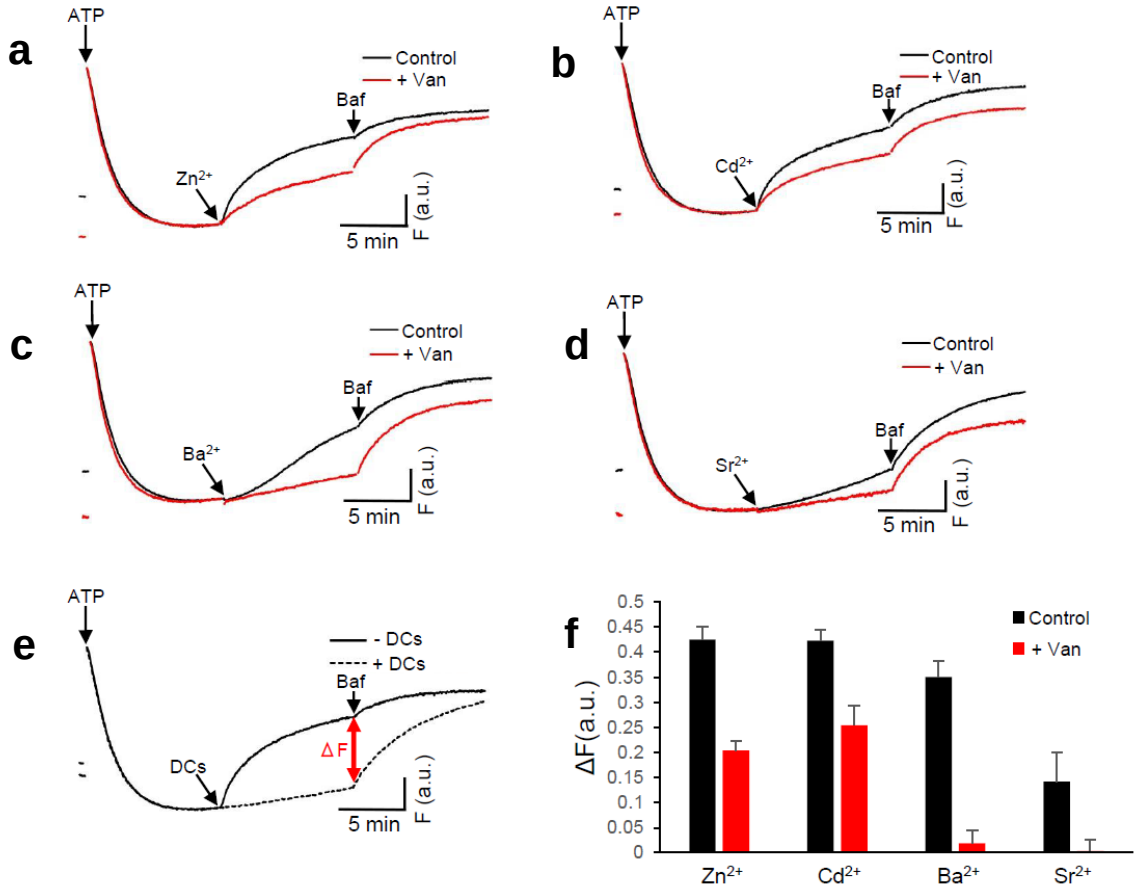

Figure 3-9 Contribution of PMCAs to divalent cations/H^+ exchange.

Effects of vanadate (Van, 500 μM) on divalent cations (DCs)-induced alkalization. Vesicles were pre-acidified in the presence of 5 mM glutamate and 3 mM KCl in the absence (black) and presence (red) of 500 μM Van, and 50 μM **(a)** $ZnCl_2$, **(b)** $CdCl_2$, **(c)** $BaCl_2$ or **(d)** $SrCl_2$ were added to induce alkalization. Since vanadate slightly reduced AO quenching signals in the presence of 5 mM glutamate and 3 mM KCl, fluorescence traces were normalized by amplitudes of acidification. All traces are the representative data from three measurements in each condition. To quantitate effects of the vanadate on divalent cations (DCs)-induced alkalization, the magnitudes of the alkalization with or without the vanadate were estimated. An example of the magnitudes, ΔFs, was indicated in a graph **(e)**. The amplitudes in each condition were summarized in **(f)**. Error bars indicate s.e.m. of three independent measurements.

3.5 The PMCAs, but not SV2s, are responsible for the majority of Ca^{2+} transport into SVs at neutral pH

To verify if Ca^{2+}-induced alkalization observed in my assay conditions was correlated with Ca^{2+} transport by PMCAs, I next examined radioactive $^{45}Ca^{2+}$ uptake in the presence of various inhibitors. For this purpose, LP2 fraction was further purified by applying it to sucrose gradient centrifugation to minimize the contamination of other organelles and membranes. Consistent with the previous report [62], $^{45}Ca^{2+}$ uptake was suppressed by PMCA inhibitors (10 μM eosin and 500 μM vanadate) to background levels measured in the absence of ATP (Figure 3-10a). In contrast, the V-ATPase inhibitor, bafilomycin (500 nM), did not affect $^{45}Ca^{2+}$ uptake (Figure 3-10b). Collectively, these results indicate that PMCAs are responsible for the majority of Ca^{2+} transport into SVs. In agreement with the results from acidification assays using SV2-KO vesicles, $^{45}Ca^{2+}$ uptake into SVs derived from SV2A/SV2B-DKO mice (which lack the majority of SV2 proteins) was not significantly different from that derived from wild-type mice (Figure 3-10c). Likewise, addition of 30 μM LEV did not reduce Ca^{2+} transport into SVs derived from SV2B/2C-DKO mice (Figure 3-10d), excluding the possibility that SV2s play a role in Ca^{2+} transport into SVs.

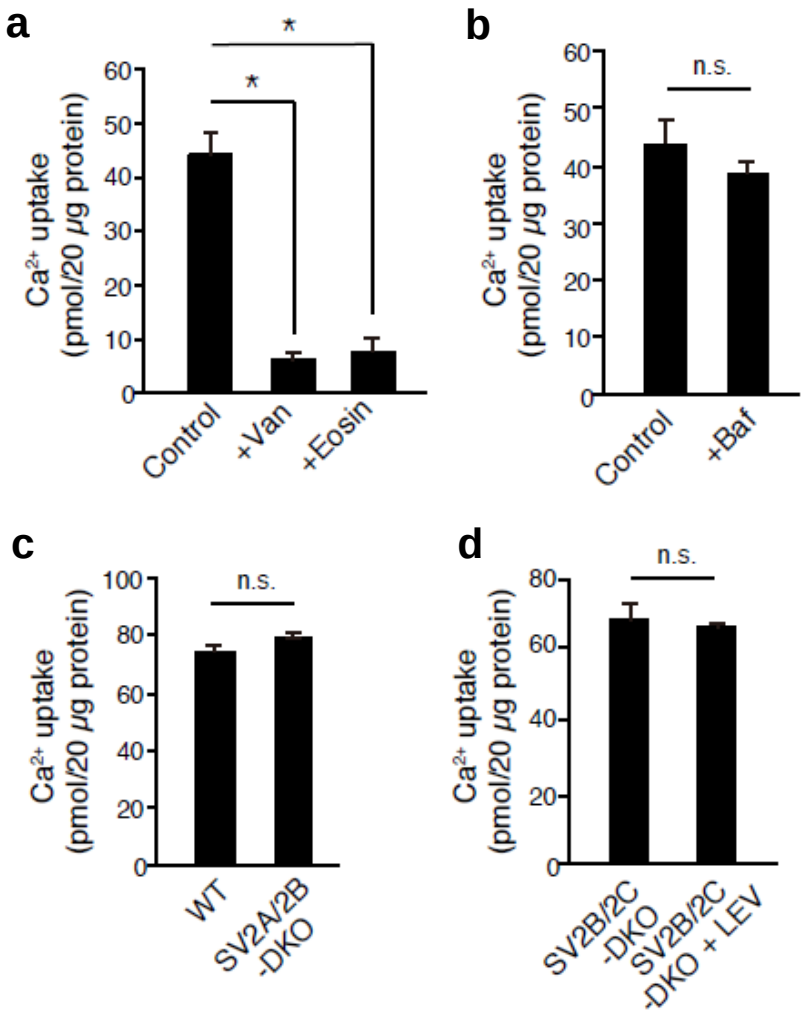

Figure 3-10 PMCAs predominantly contribute to Ca^{2+} uptake into SVs independent of H^+ electrochemical gradient generated by V-ATPase.

(a) Ca^{2+} transport was measured using $^{45}Ca^{2+}$ as a tracer. The assay was performed in the absence of inhibitors (Control) or in the presence of vanadate (Van, 500 µM) or eosin (10 µM). Both PMCA blockers effectively inhibited Ca^{2+} transport into the SV fraction. Error bars indicate s.e.m. of three independent measurements. *p < 0.0025, unpaired equal variance Student's *t*-test.

(b) Ca^{2+} transport was measured as in (a) in the absence (Control) and presence of the V-ATPase inhibitor, bafilomycin A (500 nM) (Baf). Error bars indicate s.e.m. of three measurements. n.s. indicates not significant (p > 0.1, unpaired equal variance Student's *t*-test).

(c) Ca^{2+} transport into LP2 from wild-type mice (WT) and that from SV2A/2B-DKO mice were measured. Error bars indicate s.e.m. of three measurements. n.s. indicates not significant ($p > 0.1$, unpaired equal variance Student's *t*-test).
(d) Ca^{2+} transport into LP2 from SV2B/2C-DKO mice in the absence or presence of 30 μM levetiracetam (LEV) were compared. Error bars indicate s.e.m. of three measurements. n.s. indicates not significant ($p > 0.1$, unpaired equal variance Student's *t*-test).

3.6 PMCA1-pHluorin localizes in acidic compartments at presynaptic terminals

The biochemical data described have demonstrated that PMCAs were responsible for the majority of Ca^{2+} transport into SV-rich membrane fractions, but it remains unclear whether they localized in functionally competent SVs in living neurons. In fact, isolated SVs from rodent brains contain various endosomal proteins such as endosomal SNAREs and rab proteins that may preferentially localize non-recycling vesicles at presynaptic terminals [7]. To clarify whether PMCAs localized at recycling or non-recycling vesicles in living neurons, I constructed a fluorescent reporter in which a pH-sensitive green fluorescent protein (super-ecliptic pHluorin; SEP [99]) was conjugated to the first luminal loop of PMCA1 (Figure 3-11a). A SEP fused to the second luminal loop of synaptophysin (SypHy) and a SEP fused to the C-terminal end of Syntaxin1a (Syntaxin1a-SEP) were used as controls for SV residents and plasma membrane residents, respectively (Figure 3-11a). Due to the pH sensitivity of the reporter, fluorescence is quenched in acidic compartments whereas it rises when the reporter is exposed to the neutral pH solution in the extracellular space [99]. When PMCA1-SEP was transiently expressed in cultured hippocampal neurons derived from embryonic mouse brains, immunostaining of the fixed cells with an anti-GFP antibody revealed ubiquitous expression of PMCA1-SEP in cell bodies and

dendrites (Figure 3-11b, left), as well as in presynaptic bouton-like structures (Figure 3-11b, right).

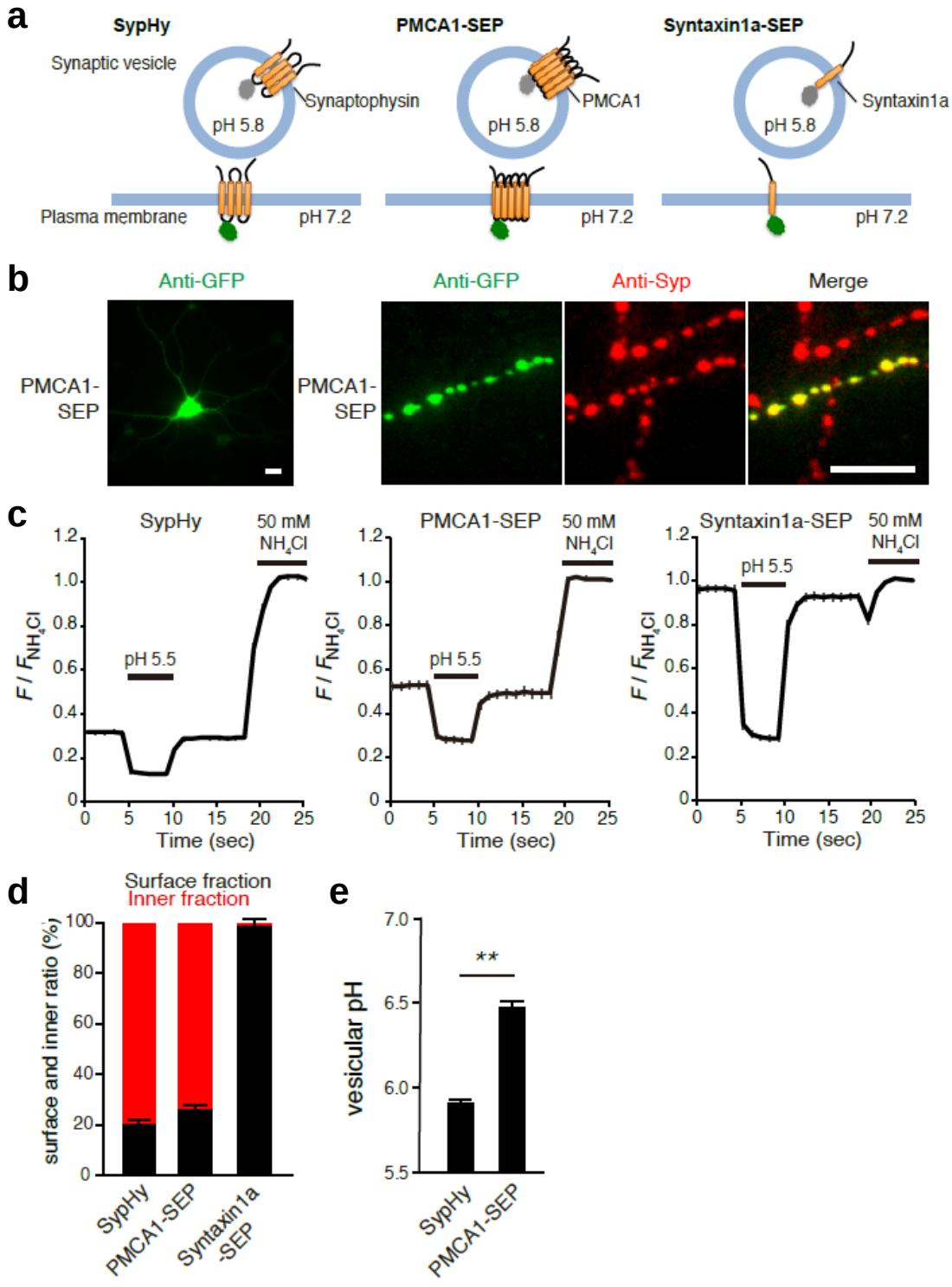

Figure 3-11 Localization of PMCA1-pHluorin in acidic compartments at presynaptic terminals of cultured hippocampal neurons.

(a) Schematic diagrams of the pHluorin probes. The super-ecliptic pHluorin (SEP) was fused either to the second luminal loop of synaptophysin (SypHy), to the first luminal loop of PMCA1 (PMCA1-SEP), or to the C-terminal end of syntaxin1a (Syntaxin1a-SEP). When these proteins reside on synaptic vesicle membranes, the SEP fluorescence is quenched due to the acidic pH (~5.8), whereas they become fluorescent when they are present at the plasma membrane and are thereby exposed to the extracellular neutral pH (~7.2).

(b) Fluorescence images of cultured hippocampal neurons expressing PMCA1-SEP. PMCA1-SEP was visualized by immunostaining with rabbit polyclonal anti-GFP antibody (green). A synaptic vesicle marker, synaptophysin, was visualized by immunostaining with mouse monoclonal anti-synaptophysin antibody (red). The right panels show merged pictures of the two immunostainings. Scale bars indicate 10 μm (cell body in the left panel) and 5 μm (right panels).

(c) Average fluorescence of SypHy (left, n = 100 boutons from 10 images), PMCA1-SEP (middle, n = 99 from 10 images), and Syntaxin1a-SEP (right, n = 100 from 10 images) in response to sequential application of a pH 5.5 solution and 50 mM NH_4Cl. After baseline subtraction, fluorescence of bouton-like structures were normalized to those during 50 mM NH_4Cl application.

(d) Distribution of SypHy and PMCA1-SEP between cell surface (black bars) and acidic intracellular compartment (red bars) deduced from the traces in (c). Error bars indicate s.e.m. for the cell surface fraction.

(e) Luminal pHs of vesicles carrying SypHy or PMCA1-SEP deduced from the traces in (c). Error bars indicate s.e.m. ** $p < 0.00025$, unpaired unequal variance Student's *t*-test.

Co-immunostaining with an antibody against synaptophysin further confirmed the presynaptic localization of PMCA1-SEP (Figure 3-11b, right panels). Estimation of inner/surface distribution of PMCA1-SEP by sequential applications of an acidic solution (pH 5.5) and a 50 mM NH_4Cl solution [100] indicated that ~75% of PMCA1-SEP was localized in the acidic compartments whose

average pH was 6.47 ± 0.03 (Figure 3-11d,e, Figure 3-12).

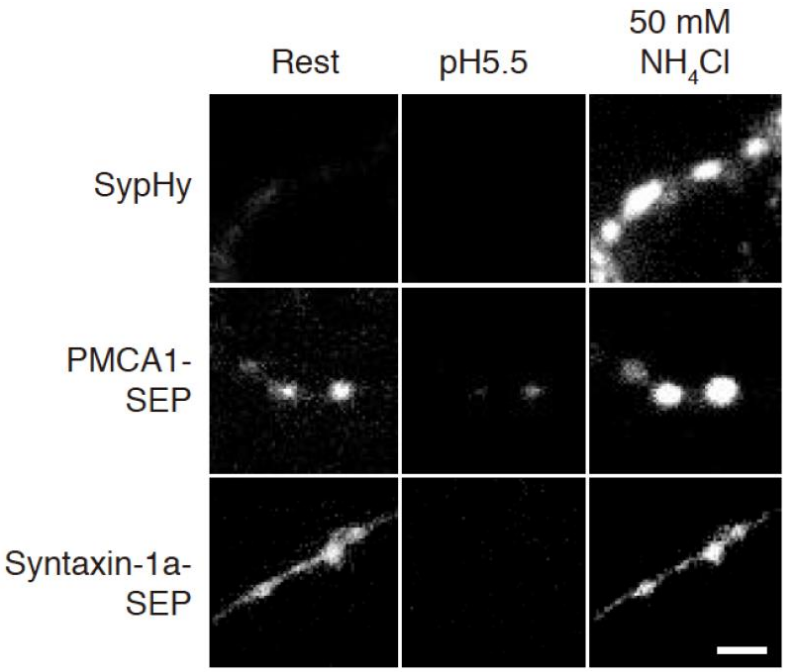

Figure 3-12 Localization of PMCA1-pHluorin, SypHy and Syntaxin-1a-SEP in acidic compartments at presynaptic terminals of cultured hippocampal neurons.
Representative images of SypHy (upper panels), PMCA1-SEP (middle panels), and Syntaxin1a-SEP (lower panels) at resting condition (left), during acid (middle), and 50 mM NH_4Cl (right) application. Scale bar indicates 10 μm.

Control experiments with SypHy revealed that ~80% of SypHy was localized in the acidic compartments whose average luminal pH was ~5.91 ± 0.02. In contrast, control experiments with Syntaxin1a-SEP revealed that it was localized almost exclusively on the plasma membrane (99.5 ± 2.2%) (Figure 3-11c-e, Figure 3-12). The higher luminal pH of PMCA1-pHluorin-positive vesicles indicates that a portion of PMCA1-pHluorin may localize in endosomal compartments.

Alternatively, exogenous expression of PMCA1-pHluorin may exert additional Ca^{2+}/H^{+} antiport, which would facilitate alkalization of the vesicular lumen. Collectively, although PMCA1-SEP expression was not restricted to the presynaptic terminals in cultured hippocampal neurons, a fraction of PMCA1-SEP did seem to be localized in the acidic compartments whose luminal pH was similar to that of typical SVs.

3.7 PMCA1-SEP recycles at presynaptic terminals

To examine whether PMCA1-SEP-positive vesicles would recycle at presynaptic terminals in an activity-dependent manner, cultured hippocampal neurons expressing PMCA1-SEP were exposed to repetitive electrical stimulation (Figure 3-13). At the end of recordings, 50 mM NH_4Cl solution was applied to estimate the total fluorescence of the SEP molecules (Figure 3-13a). Notably, PMCA1-SEP fluorescence increased upon repetitive stimulation at 20 Hz for 10 sec in a manner similar to that of SypHy (Figure 3-13a), although the fraction of PMCA1-SEP molecules engaged in exocytosis during stimulation was significantly less than that of SypHy (Figure 3-13b). In accordance with the slightly higher vesicular pH of the PMCA1-carrying vesicles (Figure 3-11e), this indicated that compared to synaptophysin, more PMCA1 was localized in non-recycling acidic compartments such as endosomes. The kinetics of the rise phase (mainly reflecting exocytosis) and decay phase (reflecting endocytosis and subsequent re-acidification of endocytosed vesicles) were identical to those of SypHy ((Figure 3-13c-e). Furthermore, when neurons were treated with 10 nM tetanus toxin (TeNT), which cleaves the major vesicular SNARE (v-SNARE) synaptobrevin/VAMP2 [101], PMCA1-SEP responses were completely abolished (Figure 3-13f, Figure 3-14). This effect was also observed for SypHy

(Figure 3-13f, Figure 3-14), indicating that PMCA1 was present on synaptobrevin/VAMP2-positive vesicles and followed the same fate as that of synaptobrevin/VAMP2 during activity-dependent SV recycling.

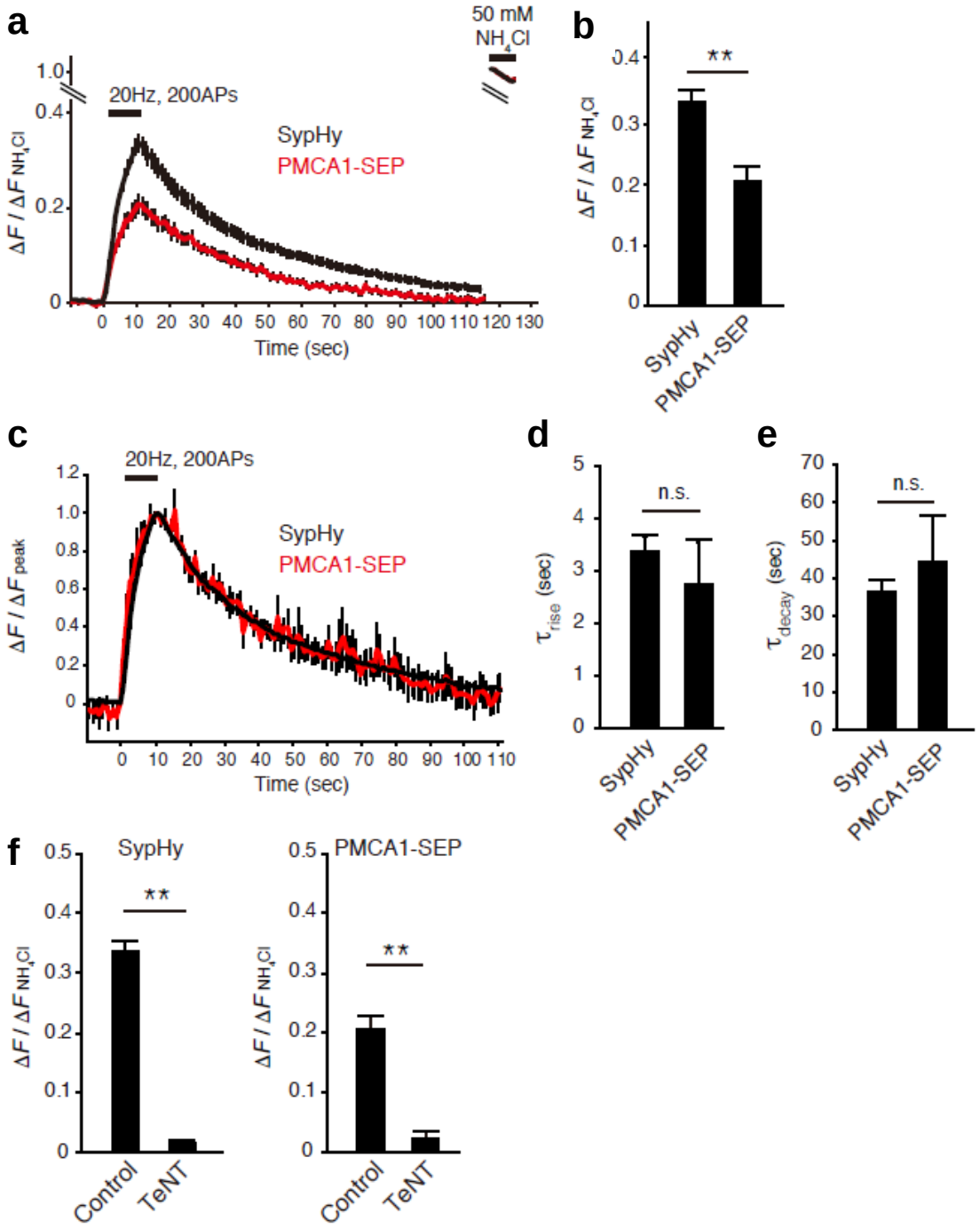

Figure 3-13 Activity-dependent recycling of PMCA1-pHluorin at presynaptic terminals.

(a) SypHy (black; n = 100 boutons from 10 images) and PMCA1-SEP (red; n = 53 from 6 images) fluorescence in response to 200 action potentials (APs) at 20 Hz. Fluorescence signals were normalized to those obtained during NH_4Cl application at the end of recordings.

(b) Peak fluorescence of SypHy and PMCA1-SEP at the end of field stimulation. Error bars indicate s.e.m. ** $p < 0.00025$, unpaired unequal variance Student's *t*-test.

(c) Superimposed traces of SypHy (black) and PMCA1-SEP (red). The traces in (a) were normalized to the peak fluorescence at the end of repetitive stimulation.

(d) Time constants of the rise time during stimulation. Exocytic rise phases were fitted with single exponentials and time constants (τ_{rise}) were deduced by using the Solver function in Excel software. An average from one image was taken as n =1. Error bars indicate s.e.m. n.s indicates $p > 0.1$, unpaired equal variance Student's *t*-test.

(e) Time constants of the decay phases after the cessation of stimuli. Decay traces were fitted with single exponentials and endocytic time constants (τ_{decay}) were deduced using the Solver function in Excel software. An average from one image was taken as n =1. Error bars indicate s.e.m. n.s indicates $p > 0.1$, unpaired equal variance Student's *t*-test.

(f) SypHy (left; n = 88 boutons from 9 images) and PMCA1-SEP (right; n = 72 boutons from 8 images) fluorescence in response to 200 APs at 20 Hz without (Control) or with 16 hours tetanus toxin treatment (TeNT, 10 nM). Bars indicate peak fluorescence of SypHy and PMCA1 at the end of stimulation with or without tetanus toxin pretreatment. Error bars indicate s.e.m. ** $p < 0.00025$, unpaired unequal variance Student's *t*-test.

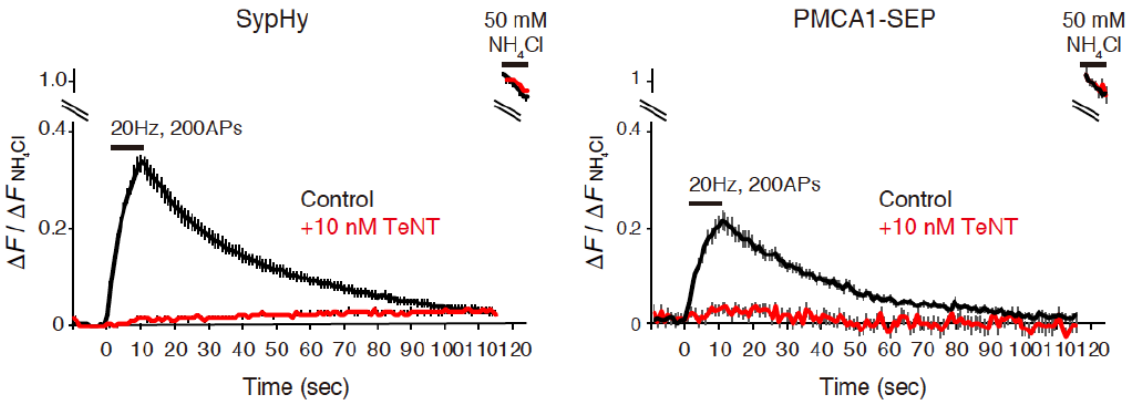

Figure 3-14 Activity-dependent recycling of PMCA1-pHluorin at presynaptic terminals with or without TeNT.

Average traces of SypHy (left) and PMCA1-SEP (right) in control (black) and after treatment with 10 nM TeNT (red). Neurons were subjected to 20 Hz stimulation for 10 s. Fluorescence was normalized to that in the presence of 50 mM NH_4Cl at the end of the recordings.

4. Discussion

In this study, I characterized the biochemical properties of Ca^{2+} transport into SVs isolated from rodent brains. I found that PMCAs, the plasma membrane Ca^{2+} ATPases, confer the majority of Ca^{2+} transport into SVs. Previous studies have indicated that there are two Ca^{2+} transport systems in isolated SVs; one is mediated by PMCAs at neutral pH, and the other is mediated by an independent Ca^{2+}/H^{+} exchanger at alkaline pH. My results strongly support a united model indicating that PMCAs are solely responsible for both activities in the majority of the SV population at neutral pH. Novel findings extending beyond those of previous studies [62,85,86,91] are as follows. First, even at neutral pH of the extra-vesicular space, Ca^{2+} alkalized pre-acidified SV lumen. This phenomenon became evident when BAPTA was used to control free Ca^{2+} concentrations, although I currently do not understand why the use of EGTA attenuated alkalization signals in the acidification assays. Since the SV alkalization by Ca^{2+} was restored by vanadate which concomitantly impeded ^{45}Ca uptake into SVs, I conclude that PMCAs are responsible for Ca^{2+}/H^{+} exchange activity. This is consistent with more recent findings that counter transport of H^{+} is associated with Ca^{2+} transport by PMCAs [102]. Second, the Ca^{2+}/H^{+} exchange at neutral pH exhibited high affinity for Ca^{2+} (K_m ~ 400 nM) that was similar to the reported values for PMCAs [103], whereas previously reported Ca^{2+}/H^{+} exchange activity at alkaline pH was characterized as a low affinity Ca^{2+}/H^{+} exchanger ($K_{0.5}$ ~ 217 μM) [62]. Third, although PMCAs have been characterized as residing in the plasma membrane, my imaging analysis revealed that PMCAs were potentially capable of recycling in an activity-dependent manner at presynaptic terminals. This observation was further substantiated by the fact that recycling of

PMCA1-SEP depended exclusively on the presence of synaptobrevin/VAMP2 on the same vesicles, which is essential for stimulus-dependent exocytosis of SVs [104].

My results are highly consistent with biochemical evidence that, in addition to V-type H^+ ATPases, vanadate-sensitive P-type ATPases constitute the major ATPases in cholinergic SVs from Torpedo electric organs [105] as well as clathrin-coated vesicles from bovine brains [106]. Although PMCAs, which are P-type ATPases, have been characterized as plasma membrane residents, my results demonstrate that PMCAs constitute the major ATPase on recycling SVs as well. This is also consistent with proteomic analyses that identified PMCAs within SV fractions [7,107]. Thus, besides the main role of PMCAs in excluding Ca^{2+} from the presynaptic cytosol to the extracellular space at the plasma membrane, vesicular PMCAs may also contribute to Ca^{2+} clearance from the presynaptic cytosol. Furthermore, since Ca^{2+} transport into SVs is coupled to H^+ efflux, vesicular PMCAs may be involved in the regulation of $\Delta\mu H^+$ of SVs, which drives neurotransmitter uptake into SVs. Indeed, external (cytosolic) Ca^{2+} strongly inhibited dopamine uptake into isolated SV fraction [108], which is reasonable given that ΔpH, the driving force for dopamine uptake, is attenuated by Ca^{2+}/H^+ exchange. In contrast, glutamate uptake, which is predominantly driven by $\Delta\Psi$, was only marginally facilitated under the condition where $\Delta\Psi$ predominated in the presence of 4 mM Cl^- [108]. However, since these dopamine and glutamate uptake assays are performed at alkaline pH of 8.5, it is necessary to perform the uptake assay at physiological pH for the more detailed evaluation of the effect of vesicular PMCA on $\Delta\mu_{H+}$.[54,102,108-111]

The plasma membrane PMCAs are responsible for transient acidification of the cytoplasm during sustained stimulation at mouse motor nerve terminals, which may regulate endocytosis [112].

My imaging analysis indicated that a substantial portion of vesicular PMCAs are inserted into the plasma membrane by exocytosis and retained there until endocytosis is completed, indicating that the total PMCA expression on the plasma membrane increases, especially during high activity. Although the contribution of the vesicular PMCAs that are inserted into the plasma membrane to acidification of the cytoplasm seems to be negligible [112], it remains to be determined to what extent Ca^{2+} extrusion from the cytoplasm is accelerated by the vesicular PMCAs that translocate into the plasma membrane during high neural activity.

In mammals, four different genes encode the four isoforms of PMCA [113]. PMCA1 and PMCA4 are expressed ubiquitously, whereas PMCA2 and PMCA3 are expressed predominantly in the central nervous system. Furthermore, each isoform has multiple splice variants, comprising more than 30 spliced isoforms, although little is known about the functional significance of multiple splice variants [113]. In this study, I show that one of the PMCAs, the full length PMCA1 (1,249 a.a.) fused to pHluorin at its luminal region, is sorted preferentially to recycling SVs rather than to the plasma membrane at presynaptic terminals, and its distribution and recycling behaviors are very similar to those of the SV marker, synaptophysin (Figure 3-11 and Figure 3-13). It remains unknown whether other PMCA isoforms or respective splice variants show similar properties to those of the full length PMCA1-pHluorin at presynaptic terminals, which may necessitate more complex regulation of Ca^{2+} and H^{+} dynamics at presynaptic terminals. Additionally, it should be kept in mind that I still lack concrete evidence for the existence of PMCA proteins on SVs, as the evidence I provide in this study relies on the usage of pharmacological blockade of Ca^{2+} transport by PMCA blockers and also on the exogenous expression of PMCA1 fused to fluorescent proteins. Although the SV proteome supports the

existence of PMCA in the SV fraction isolated from native brains [7], previous fractionation experiments, combined with western blot analysis using isoform-specific PMCA antibodies, have provided controversial results concerning the localization of PMCA isoforms in synaptic vesicles [108,113], probably due to their predominant expression at the plasma membrane of the cell body. Thus, direct demonstration of PMCA isoforms on synaptic vesicles, e.g. via immuno-gold labeling of isolated SV fractions or immuno-gold labeling of brain sections, will be essential to confirm their vesicular localization in the future.

For the clearance of the Ca^{2+} in presynaptic axon terminals, several distinct mechanisms have been suggested: PMCA, SERCA, Na^+/Ca^{2+} exchanger and mitochondria. Previous fluorescent Ca^{2+} imaging, combined with the whole-cell patch-clamp techniques upon the blockade of each Ca^{2+} clearance system at the calyces of Held of rat brains, have revealed the contribution of PMCA (23%), K^+-dependent Na^+/Ca^{2+} exchanger (42%), K^+-independent Na^+/Ca^{2+} exchanger (26%) and SERCA (~0%) in response to small Ca^{2+} transients (< 2 μ M)[114]. Moreover, Kim et al. suggested that mitochondria also contributed to a larger extent when the Ca^{2+} load to the calyx of the Held was larger or prolonged[114]. Despite these observations[114], the contribution of the vesicular PMCAs is still elusive, because the PMCA blockers, such as vanadate and carboxyeosin, are membrane-permeable and block all the PMCAs not only on synaptic vesicles but also on the plasma membrane in fluorescent Ca^{2+} imaging.

Ca^{2+} plays a key role in signal transduction not only in neurons but also in various cell types. For instance, in pancreatic β-cells, which are one of the endocrine cells and release insulin for glucose homeostasis in the blood, the secretion of the insulin is regulated by the concentration of the Ca^{2+}. The PMCAs participates in the Ca^{2+} clearance of these cells in a similar manner to that

of presynaptic terminals. Using fluorescent Ca^{2+} imaging, Chen et al. suggested that the contribution of all PMCAs to Ca^{2+} clearance at the pancreatic β-cell accounts for 21-27%[115], which is similar to the contribution of the PMCAs at the presynaptic bouton[114]. However, in contrast to the presynaptic bouton, in pancreatic the β-cell, mitochondrial Ca^{2+} uptake contributed little, Na^+/Ca^{2+} exchanger is not major Ca^{2+} clearance system (21-30%) and SERCA pump is the major Ca^{2+} clearance system (50-64%)[115]. Hence, the PMCA may be the common Ca^{2+} clearance system including synaptic boutons and the endocrine cells. On the other hand, the activation of the mitochondrial Ca^{2+} uptake and Na^+/Ca^{2+} may leads to short-lasting secretion observed in the synaptic boutons but not in endocrine cells such as the pancreatic β-cells.[115]

SV2s have been postulated to function as a Ca^{2+} transporter, since synaptic phenotypes observed in SV2-deficient mice could be well explained if SV2s function as Ca^{2+} transporters [69,70]. However, my results from direct tests of Ca^{2+} transport into SV2-deficient vesicles rule out this hypothesis (Figure 3-6 and Figure 3-10). Therefore, the Ca^{2+}-related phenotypes observed previously in SV2-deficient mice may be indirect consequences of unknown functions of SV2. Of note, it has recently been shown that SV2A mediates galactose/H^+ symport when heterologously expressed in yeast cells [116]. Although the functional significance of galactose in the nervous system, particularly its role in SVs, has been enigmatic, changes in either metabolism of carbohydrates or composition of glycans attached to proteins or lipids may indirectly regulate Ca^{2+} homeostasis at presynaptic terminals, which would lead to the observed Ca^{2+}-related phenotypes in SV2-deficient synapses. Uncovering the link between SV2s' function and presynaptic [Ca^{2+}] regulation will help to elucidate the role of SV2s in epileptogenesis caused by SV2A gene knockout [69,117].

In summary, my present results collectively suggest that Ca^{2+} transport across SV membranes is predominantly, if not exclusively, mediated by PMCAs. Due to their property as Ca^{2+}/H^{+} exchangers, PMCAs may contribute to the regulation of $\Delta\mu H^{+}$ and the dynamic control of cytosolic Ca^{2+} (Figure 4-1) and H^{+} at presynaptic terminals. Since various single nucleotide polymorphisms (SNPs) have been identified in PMCA genes that are associated with neuronal disorders such as autism and deafness [118], it will be crucial to establish how these SNPs affect the function and distribution of PMCAs in neurons to elucidate the mechanisms underlying these diseases.

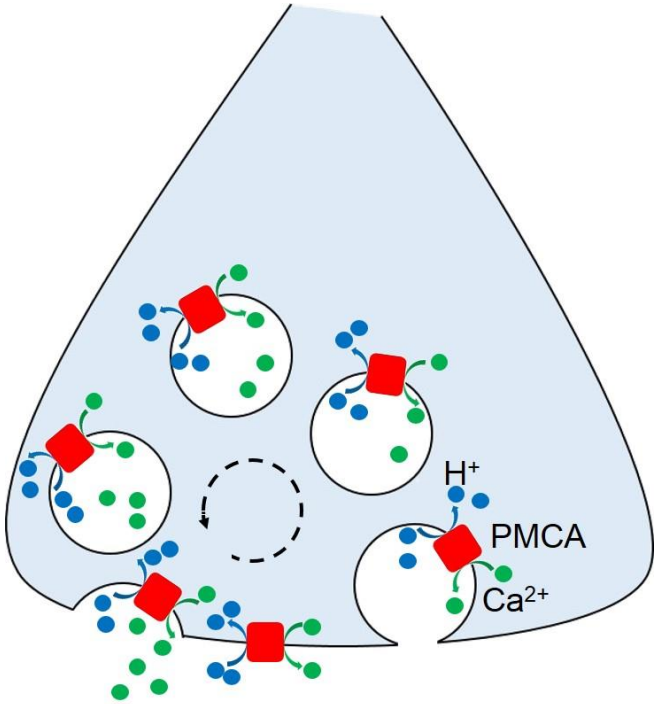

Figure 4-1 Ca^{2+} clearance model mediated by SVs at presynaptic bouton.
PMCAs (red square) are localized not only at the plasma membrane but also at SVs and exchange Ca^{2+} (green circle) with H^{+} (blue circle). Therefore, SVs (white circle) sequesters intracellular Ca^{2+} using PMCAs during the synaptic vesicle recycling.

5. Appendix

Estimation of the overall apparent association constant,*K'*

The multiple protonation sites of BAPTA and ATP must be taken in consideration in description of calcium and magnesium ion affinities. BAPTA has a total of six possible protonation sites. Around physiological pH all four carboxyl groups can be considered unprotonated, since they are highly acidic below p*Ka*s 3.26 (see https://web.stanford.edu/~cpatton/xlsconstants.htm). Similarly, whether ATP has a total of four possible protonation sites, around physiological pH firstly and thirdly phosphate of ATP can be unprotenated because they are highly acidic below p*Ka*s 0.5 (see https://web.stanford.edu/~cpatton/xlsconstants.htm). The diprotonated form of BAPTA and ATP has a negligible affinity for metal ions, and its metal ion affinity will not be considered further. Metal ion binding is then a function of binding to the unprotonated and monoprotonated spicies. The goal of the following derivation is to derive an equation for the overall apparent association constant,*K'*, in terms of absolute association constants, *K*, which are determined for standard conditions.

If only one species of BAPTA or ATP (also referred to here as ligand L) bound metal ion, the association constant would be

$$K = \frac{[\text{metal-ligand complex}]}{[\text{metal ion}][\text{chelator not bound}]} = \frac{[\text{MeL}]}{[\text{Me}][\text{L}]} . \quad [1]$$

The overall apparent association constant, K', for metal ion binding of a ligand present as several forms in solution is defined similarly as if the ligand existed as a single molecular species.

However, in determining a single value for overall apparent association constant, binding of metal ion to each form of the ligand must be taken into account.

The total amount of ligand not bound to metal is the sum of the free ligand in all its states: $L_{tot} - MeL_{tot}$. Since I consider only metal ion binding to unprotonated and monoprotonated species around physiologic pH, the following mass balance equations can be written:

$$[L_{tot}]=[L] + [HL] + [H_2L] + [MeL] + [MeHL],$$

$$[MeL_{tot}] = [MeL] + [MeHL],$$

and

$$[L_{tot} - MeL_{tot}] = [L] + [HL] + [H2L] = [L]_{free}. \quad [2]$$

Equation can then be set up for the apparent association constants of two relevant species MeL and MeHL. The notation $K'_{Me/MeL}$ represents the apparent association constant for the equation $Me + L_{free} \rightleftharpoons MeL$.

$$K'_{Me/MeL} = \frac{[MeL]}{[Me][L_{tot} - MeL_{tot}]} \quad [3]$$

$$K'_{Me/MeHL} = \frac{[MeHL]}{[Me][L_{tot} - MeL_{tot}]} \quad [4]$$

Since the overall association constant represents the sum of metal ion binding to each of these forms,

$$K' = K'_{Me/MeL} + K'_{Me/MeHL} = \frac{[MeL] + [MeHL]}{[Me][L_{tot} - MeL_{tot}]} = \frac{[MeL_{tot}]}{[Me][L_{tot} - MeL_{tot}]} . \quad [5]$$

To calculate the overall *K'* from published thermodynamic data, the above expression must be expressed in terms of the absolute association constants *K* instead of *K'*. In a comparison of the equations for the absolute and apparent association constants,

$$K_{\mathrm{Me/MeL}} = \frac{[\mathrm{MeL}]}{[\mathrm{Me}][\mathrm{L}]} \quad \text{and}$$

$$K'_{\mathrm{Me/MeL}} = \frac{[\mathrm{MeL}]}{[\mathrm{Me}][\mathrm{L_{tot}} - \mathrm{MeL_{tot}}]}$$

$$K'_{\mathrm{Me/MeHL}} = \frac{[\mathrm{MeHL}]}{[\mathrm{Me}][\mathrm{HL}]} \quad \text{and}$$

$$K'_{\mathrm{Me/MHeL}} = \frac{[\mathrm{MeHL}]}{[\mathrm{Me}][\mathrm{L_{tot}} - \mathrm{MeL_{tot}}]} \quad ,$$

it is obvious that each differs by only a single term in the denominator. Solving $K_{\mathrm{Me/MeL}}$ and $K'_{\mathrm{Me/MeL}}$ for [MeL] and equating the solutions, and doing the same for $K_{\mathrm{Me/MeHL}}$ and $K'_{\mathrm{ME/MeHL}}$, I can derive the conservation equations

$$K'_{\mathrm{Me/MeL}} = \frac{K_{\mathrm{Me/MeL}}[\mathrm{L}]}{[\mathrm{L_{tot}}\text{-}\mathrm{MeL_{tot}}]} \quad [6]$$

$$K'_{Me/MHeL} = \frac{K_{\mathrm{Me/MeHL}}[\mathrm{HL}]}{[\mathrm{L_{tot}}\text{-}\mathrm{MeL_{tot}}]} \quad . \quad [7]$$

From Eq. [2], the equation for be overall apparent association constant can be written as

$$\mathrm{K'} = \frac{\mathrm{K_{Me/MeL}}[\mathrm{L}]}{[\mathrm{L}] + [\mathrm{HL}] + [\mathrm{H_2L}]} + \frac{\mathrm{K_{Me/MeHL}}[\mathrm{HL}]}{[\mathrm{L}] + [\mathrm{HL}] + [\mathrm{H_2L}]} \quad . \quad [8]$$

[HL] and [H_2L] can be expressed in terms of values [H] and [L] and the equilibrium constant for the protonation of the ligand:

$$[\mathrm{HL}] = \mathrm{K_{H/HL}}[\mathrm{H}][\mathrm{L}]$$

$$[\mathrm{H_2L}] = \mathrm{K_{H/HL}K_{H/H2L}}[\mathrm{H}]^2[\mathrm{L}] \quad .$$

Inserting these solutions where appropriate and factoring out [L] or [HL] from the numerator and denominator, I obtain:

$$K' = \frac{K_{\mathrm{Me/MeL}}}{1 + \mathrm{K_{H/HL}}[\mathrm{H}] + \mathrm{K_{H/H2L}}[\mathrm{H}]^2} + \frac{K_{\mathrm{Me/MeHL}}}{1/(\mathrm{K_{H/HL}}[\mathrm{H}]) + 1 + \mathrm{K_{H/H2L}}[\mathrm{H}]} \quad . \quad [9]$$

This equation for overall apparent association constant is applicable around physiologic pH.

In fact, when the overall apparent association constant is calculated from Eq. [9], it is necessary to convert absolute associate constants, *K* (Table 5-1), which are determined for standard conditions, into corrected absolute associate constants, *K*, which is applicable to the experimental conditions. Absolute association constants are typically published at a given ionic strength (frequently 20 °C and 0.1 M ionic strength). This means the constants must be corrected when different conditions are used.

Using a semiempirical form of the Debye-Hükel limiting law, the individual association constants (i.e. those for $K_{MeL/MeL}$, $K_{Me/MeHL}$, etc.) are corrected for use at the desired ionic strength. The equation which allows the conversion is

$$\log K_f = \log K_i + 2xy\left(\log f_j - \log f'_j\right) . \quad [10]$$

K_i is the initial constant prior to correction, and K_f is the constant after correction. *x* and *y* refer to the charge on the cation and anion of the binding species: in this case, the charge on the metal cation and the charge on the BAPTA or ATP, taking into account its protonation state. f_j is the activity coefficient of the BAPTA or ATP at the initial ionic strength and f'_j that for the desired condition:

$$\log f_j = A\left[\left(I_e^{1/2}/\left(1+I_e^{1/2}\right)\right) - bI_e\right] . \quad [11]$$

I_e is the ionic equivalent used instead of ionic strength because it was found empirically to agree better with data. $I_e = \frac{1}{2}\sum c_j z_j$. *b* is an empiric factor which equals 0.25 for the ionic composition of buffers such as those describe here. *A* is constant given by

$$A = 1.8246 \times 10^6/(\varepsilon T)^{3/2} . \quad [12]$$

T is the absolute temperature and ε is the dielectric constant for water. $\varepsilon = 87.740 - 0.4008\,(T - 273) + 9.398\,(10^{-4})\,(T - 273)^2 - 1.410\,(10^{-6})\,(T - 273)^3$ [119]. The dielectric constant changes with temperature. In my thesis I put $\varepsilon = 79.3$ as previously reported [79] because the value of ε calculated using the equation for the derivation of ε had little effect on the calculation of the overall association constants.

After the correction for an ionic strength using [10], the constants involving hydrogen ion (i.e. those for $K_{H/HL}$, $K_{H/H2L}$, $K_{Me/MeHL}$, etc.) must be corrected for the proton activity coefficient in order to calculating the overall association constant using [9]. The equation which allows the conversion is

$$\log K_f = \log K_i - \log \gamma_i \quad . \quad [13]$$

γ_1 is the activity coefficient of proton at the desired condition. This is derived using Davies equation:

$$\log \gamma_i = -Az_i^2 \left[\left(I_e^{1/2} / \left(1 + I_e^{1/2} \right) \right) - 0.3 I_e \right] \quad . \quad [14]$$

z_i is the valence of proton. In fact, in my thesis $\log K_f$ of the Eq. [13] was calculated roughly from the table previously reported [79], which shows the increment of versus ionic strength, since the error of the value of $\log K_f$ is had little effect on the calculation of the overall association constants.

After absolute associate constant, K, which is corrected for ionic strength using Eq. [10] and [13], the overall associate constants at published temperature conditions are derived using Eq. [9].

After the derivation of the overall associate constants, K', at experimental ionic equivalent conditions at published temperatures, the constants are necessary to be converted into the corrected overall associate constants, *K'*, which is applicable to the experimental temperatures

using the van't Hoff isochore

$$\log K_f = \log K_i - (T_i - T_f) \times (\Delta H/(2.303RT^2)) \quad . \quad [15]$$

T is absolute temperature, the gas constant, R, equals 8.314 J/degree × mol, depending on the units of ΔH (Table 5-1).

Equilibrium	log K[(a)]	ΔH[(b)]
$Ca^{2+} + BAPTA^{4-} \leftrightarrows CaBAPTA^{2-}$	6.97	13900 [J/mol]
$Mg^{2+} + BAPTA^{4-} \leftrightarrows MgBAPTA^{2-}$	1.77	53800 [J/mol]
$H^{+} + BAPTA^{4-} \leftrightarrows HBAPTA^{3-}$	6.36	
$H^{+} + HBAPTA^{3-} \leftrightarrows H_2BAPTA^{2-}$	5.47	
$Ca^{2+} + ATP^{4-} \leftrightarrows CaATP^{2-}$	3.828	2107 [cal/mol]
$Mg^{2+} + ATP^{4-} \leftrightarrows MgATP^{2-}$	2.144	4245 [cal/mol]
$H^{+} + ATP^{4-} \leftrightarrows HATP^{3-}$	6.476	
$H^{+} + ATP^{3-} \leftrightarrows H_2ATP^{3-}$	4.039	
$Ca^{2+} + HATP^{3-} \leftrightarrows HATP^{-}$	2.144	
$Mg^{2+} + HATP^{3-} \leftrightarrows HATP^{-}$	2.299	

Table 5-1 Published association constants for BAPTA and ATP, as well as the *ΔH* values for BAPTA and ATP.

(a) Association constants for BAPTA (22 ºC, I = 0.1 M) are from Tsien [87]. Values for ATP (20 ºC, I = 0.1 M) are from MAXCHELATOR (see https://web.stanford.edu/~cpatton/xlsconstants.htm).

(b) A *ΔH* value for Ca^{2+} binding to BAPTA is from Harrison & Bers [120]. A value for Mg^{2+} binding to BAPTA is from Marks & Maxfield [79]. Values for either Ca^{2+} or Mg^{2+} binding to ATP are from Wilson & Chin [121].

6. Bibliography

1 Pereda, A. E. Electrical synapses and their functional interactions with chemical synapses. *Nature reviews. Neuroscience* **15**, 250-263, doi:10.1038/nrn3708 (2014).

2 Palade, G. Electron microscope observations of interneuronal and neuromuscular synapses. *The anatomical record* **118**, 335-336 (1954).

3 Del Castillo, J. & Katz, B. Quantal components of the end-plate potential. *The Journal of physiology* **124**, 560-573, doi:10.1113/jphysiol.1954.sp005129 (1954).

4 Katz, B. & Miledi, R. Spontaneous and evoked activity of motor nerve endings in calcium Ringer. *The Journal of physiology* **203**, 689-706, doi:10.1113/jphysiol.1969.sp008887 (1969).

5 Takamori, S. Presynaptic Molecular Determinants of Quantal Size. *Frontiers in synaptic neuroscience* **8**, 2, doi:10.3389/fnsyn.2016.00002 (2016).

6 Neher, E. What is Rate-Limiting during Sustained Synaptic Activity: Vesicle Supply or the Availability of Release Sites. *Frontiers in synaptic neuroscience* **2**, 144, doi:10.3389/fnsyn.2010.00144 (2010).

7 Takamori, S. *et al.* Molecular anatomy of a trafficking organelle. *Cell* **127**, 831-846, doi:10.1016/j.cell.2006.10.030 (2006).

8 Sudhof, T. C. & Rizo, J. Synaptic vesicle exocytosis. *Cold Spring Harbor perspectives in biology* **3**, doi:10.1101/cshperspect.a005637 (2011).

9 Kaeser, P. S. *et al.* RIM proteins tether Ca2+ channels to presynaptic active zones via a direct PDZ-domain interaction. *Cell* **144**, 282-295, doi:10.1016/j.cell.2010.12.029 (2011).

10 Sudhof, T. C. Neurotransmitter release: the last millisecond in the life of a synaptic vesicle. *Neuron* **80**, 675-690, doi:10.1016/j.neuron.2013.10.022 (2013).

11 Burre, J. *et al.* Alpha-synuclein promotes SNARE-complex assembly in vivo and in vitro. *Science (New York, N.Y.)* **329**, 1663-1667, doi:10.1126/science.1195227 (2010).

12 Sharma, M., Burre, J. & Sudhof, T. C. CSPalpha promotes SNARE-complex assembly by chaperoning SNAP-25 during synaptic activity. *Nature cell biology* **13**, 30-39, doi:10.1038/ncb2131 (2011).

13 Sollner, T., Bennett, M. K., Whiteheart, S. W., Scheller, R. H. & Rothman, J. E. A protein assembly-disassembly pathway in vitro that may correspond to sequential steps of synaptic vesicle docking, activation, and fusion. *Cell* **75**, 409-418 (1993).

14 Neher, E. & Sakaba, T. Multiple roles of calcium ions in the regulation of neurotransmitter release. *Neuron* **59**, 861-872, doi:10.1016/j.neuron.2008.08.019 (2008).

15 Wan, Q. F., Nixon, E. & Heidelberger, R. Regulation of presynaptic calcium in a mammalian synaptic terminal. *Journal of neurophysiology* **108**, 3059-3067, doi:10.1152/jn.00213.2012 (2012).

16 Radhakrishnan, A., Stein, A., Jahn, R. & Fasshauer, D. The Ca^{2+} affinity of synaptotagmin 1 is markedly increased by a specific interaction of its C2B domain with phosphatidylinositol 4,5-bisphosphate. *The Journal of biological chemistry* **284**, 25749-25760, doi:10.1074/jbc.M109.042499 (2009).

17 Granseth, B., Odermatt, B., Royle, S. J. & Lagnado, L. Clathrin-mediated endocytosis is the dominant mechanism of vesicle retrieval at hippocampal synapses. *Neuron* **51**, 773-786, doi:10.1016/j.neuron.2006.08.029 (2006).

18 Saheki, Y. & De Camilli, P. Synaptic vesicle endocytosis. *Cold Spring Harbor perspectives in biology* **4**, a005645, doi:10.1101/cshperspect.a005645 (2012).

19 Alabi, A. A. & Tsien, R. W. Perspectives on kiss-and-run: role in exocytosis, endocytosis, and neurotransmission. *Annual review of physiology* **75**, 393-422, doi:10.1146/annurev-physiol-020911-153305 (2013).

20 Watanabe, S. & Boucrot, E. Fast and ultrafast endocytosis. *Current opinion in cell biology* **47**, 64-71, doi:10.1016/j.ceb.2017.02.013 (2017).

21 Clayton, E. L., Evans, G. J. & Cousin, M. A. Bulk synaptic vesicle endocytosis is rapidly triggered during strong stimulation. *The Journal of neuroscience : the official journal of the Society for Neuroscience* **28**, 6627-6632, doi:10.1523/jneurosci.1445-08.2008 (2008).

22 Wu, Y. *et al.* A dynamin 1-, dynamin 3- and clathrin-independent pathway of synaptic vesicle recycling mediated by bulk endocytosis. *eLife* **3**, e01621, doi:10.7554/eLife.01621 (2014).

23 Hayashi, M. *et al.* Cell- and stimulus-dependent heterogeneity of synaptic vesicle endocytic recycling mechanisms revealed by studies of dynamin 1-null neurons. *Proceedings of the National Academy of Sciences of the United States of America*

105, 2175-2180, doi:10.1073/pnas.0712171105 (2008).

24 Miller, T. M. & Heuser, J. E. Endocytosis of synaptic vesicle membrane at the frog neuromuscular junction. *The Journal of cell biology* **98**, 685-698 (1984).

25 Zhang, B. *et al.* Synaptic vesicle size and number are regulated by a clathrin adaptor protein required for endocytosis. *Neuron* **21**, 1465-1475 (1998).

26 Lou, X., Paradise, S., Ferguson, S. M. & De Camilli, P. Selective saturation of slow endocytosis at a giant glutamatergic central synapse lacking dynamin 1. *Proceedings of the National Academy of Sciences of the United States of America* **105**, 17555-17560, doi:10.1073/pnas.0809621105 (2008).

27 Shupliakov, O. *et al.* Impaired recycling of synaptic vesicles after acute perturbation of the presynaptic actin cytoskeleton. *Proceedings of the National Academy of Sciences of the United States of America* **99**, 14476-14481, doi:10.1073/pnas.212381799 (2002).

28 Wu, W. & Wu, L. G. Rapid bulk endocytosis and its kinetics of fission pore closure at a central synapse. *Proceedings of the National Academy of Sciences of the United States of America* **104**, 10234-10239, doi:10.1073/pnas.0611512104 (2007).

29 Watanabe, S. *et al.* Ultrafast endocytosis at mouse hippocampal synapses. *Nature* **504**, 242-247, doi:10.1038/nature12809 (2013).

30 Bai, L., Xu, H., Collins, J. F. & Ghishan, F. K. Molecular and functional analysis of a novel neuronal vesicular glutamate transporter. *The Journal of biological chemistry* **276**, 36764-36769, doi:10.1074/jbc.M104578200 (2001).

31 Fremeau, R. T., Jr. *et al.* The identification of vesicular glutamate transporter 3 suggests novel modes of signaling by glutamate. *Proceedings of the National Academy of Sciences of the United States of America* **99**, 14488-14493, doi:10.1073/pnas.222546799 (2002).

32 Fremeau, R. T., Jr. *et al.* The expression of vesicular glutamate transporters defines two classes of excitatory synapse. *Neuron* **31**, 247-260 (2001).

33 Herzog, E. *et al.* The existence of a second vesicular glutamate transporter specifies subpopulations of glutamatergic neurons. *The Journal of neuroscience : the official journal of the Society for Neuroscience* **21**, Rc181 (2001).

34 Ni, B., Rosteck, P. R., Jr., Nadi, N. S. & Paul, S. M. Cloning and expression of a cDNA encoding a brain-specific Na^+-dependent inorganic phosphate

cotransporter. *Proceedings of the National Academy of Sciences of the United States of America* **91**, 5607-5611 (1994).

35 Takamori, S., Rhee, J. S., Rosenmund, C. & Jahn, R. Identification of a vesicular glutamate transporter that defines a glutamatergic phenotype in neurons. *Nature* **407**, 189-194, doi:10.1038/35025070 (2000).

36 Takamori, S., Rhee, J. S., Rosenmund, C. & Jahn, R. Identification of differentiation-associated brain-specific phosphate transporter as a second vesicular glutamate transporter (VGLUT2). *The Journal of neuroscience : the official journal of the Society for Neuroscience* **21**, Rc182 (2001).

37 McIntire, S. L., Reimer, R. J., Schuske, K., Edwards, R. H. & Jorgensen, E. M. Identification and characterization of the vesicular GABA transporter. *Nature* **389**, 870-876, doi:10.1038/39908 (1997).

38 Sagne, C. *et al.* Cloning of a functional vesicular GABA and glycine transporter by screening of genome databases. *FEBS letters* **417**, 177-183 (1997).

39 Erickson, J. D., Eiden, L. E. & Hoffman, B. J. Expression cloning of a reserpine-sensitive vesicular monoamine transporter. *Proceedings of the National Academy of Sciences of the United States of America* **89**, 10993-10997, doi:10.1073/pnas.89.22.10993 (1992).

40 Liu, Y. *et al.* A cDNA that suppresses MPP+ toxicity encodes a vesicular amine transporter. *Cell* **70**, 539-551 (1992).

41 Wimalasena, K. Vesicular monoamine transporters: structure-function, pharmacology, and medicinal chemistry. *Medicinal research reviews* **31**, 483-519, doi:10.1002/med.20187 (2011).

42 Erickson, J. D. *et al.* Functional identification of a vesicular acetylcholine transporter and its expression from a "cholinergic" gene locus. *The Journal of biological chemistry* **269**, 21929-21932 (1994).

43 Sawada, K. *et al.* Identification of a vesicular nucleotide transporter. *Proceedings of the National Academy of Sciences of the United States of America* **105**, 5683-5686, doi:10.1073/pnas.0800141105 (2008).

44 Edwards, R. H. The neurotransmitter cycle and quantal size. *Neuron* **55**, 835-858, doi:10.1016/j.neuron.2007.09.001 (2007).

45 Maycox, P. R., Deckwerth, T., Hell, J. W. & Jahn, R. Glutamate uptake by brain synaptic vesicles. Energy dependence of transport and functional reconstitution in

proteoliposomes. *The Journal of biological chemistry* **263**, 15423-15428 (1988).

46 Naito, S. & Ueda, T. Characterization of glutamate uptake into synaptic vesicles. *Journal of neurochemistry* **44**, 99-109 (1985).

47 Hori, T. & Takahashi, T. Kinetics of synaptic vesicle refilling with neurotransmitter glutamate. *Neuron* **76**, 511-517, doi:10.1016/j.neuron.2012.08.013 (2012).

48 Ishikawa, T., Sahara, Y. & Takahashi, T. A single packet of transmitter does not saturate postsynaptic glutamate receptors. *Neuron* **34**, 613-621 (2002).

49 Yamashita, T., Ishikawa, T. & Takahashi, T. Developmental increase in vesicular glutamate content does not cause saturation of AMPA receptors at the calyx of Held synapse. *The Journal of neuroscience : the official journal of the Society for Neuroscience* **23**, 3633-3638 (2003).

50 Wojcik, S. M. *et al.* An essential role for vesicular glutamate transporter 1 (VGLUT1) in postnatal development and control of quantal size. *Proceedings of the National Academy of Sciences of the United States of America* **101**, 7158-7163, doi:10.1073/pnas.0401764101 (2004).

51 Daniels, R. W. *et al.* Increased expression of the Drosophila vesicular glutamate transporter leads to excess glutamate release and a compensatory decrease in quantal content. *The Journal of neuroscience : the official journal of the Society for Neuroscience* **24**, 10466-10474, doi:10.1523/jneurosci.3001-04.2004 (2004).

52 Takamori, S. in *Presynaptic Terminals* Ch. 12, 275-294 (2015).

53 Stobrawa, S. M. *et al.* Disruption of ClC-3, a chloride channel expressed on synaptic vesicles, leads to a loss of the hippocampus. *Neuron* **29**, 185-196 (2001).

54 Schenck, S., Wojcik, S. M., Brose, N. & Takamori, S. A chloride conductance in VGLUT1 underlies maximal glutamate loading into synaptic vesicles. *Nat Neurosci* **12**, 156-162, doi:10.1038/nn.2248 (2009).

55 Takamori, S. Vesicular glutamate transporters as anion channels? *Pflugers Archiv : European journal of physiology* **468**, 513-518, doi:10.1007/s00424-015-1760-y (2016).

56 Goh, G. Y. *et al.* Presynaptic regulation of quantal size: K^+/H^+ exchange stimulates vesicular glutamate transport. *Nat Neurosci* **14**, 1285-1292, doi:10.1038/nn.2898 (2011).

57 Preobraschenski, J., Zander, J. F., Suzuki, T., Ahnert-Hilger, G. & Jahn, R.

Vesicular glutamate transporters use flexible anion and cation binding sites for efficient accumulation of neurotransmitter. *Neuron* **84**, 1287-1301, doi:10.1016/j.neuron.2014.11.008 (2014).

58 Israel, M. *et al.* Calcium uptake by cholinergic synaptic vesicles. *Journal de physiologie* **76**, 479-485 (1980).

59 Israel, M. *et al.* ATP-dependent calcium uptake by cholinergic synaptic vesicles isolated from Torpedo electric organ. *The Journal of membrane biology* **54**, 115-126 (1980).

60 Michaelson, D. M., Ophir, I. & Angel, I. ATP-stimulated Ca^{2+} transport into cholinergic Torpedo synaptic vesicles. *Journal of neurochemistry* **35**, 116-124 (1980).

61 Parducz, A. & Dunant, Y. Transient increase of calcium in synaptic vesicles after stimulation. *Neuroscience* **52**, 27-33 (1993).

62 Goncalves, P. P., Meireles, S. M., Neves, P. & Vale, M. G. Distinction between Ca^{2+} pump and Ca^{2+}/H^{+} antiport activities in synaptic vesicles of sheep brain cortex. *Neurochemistry international* **37**, 387-396 (2000).

63 Goncalves, P. P., Meireles, S. M., Gravato, C. & Vale, M. G. Ca^{2+}-H^{+} antiport activity in synaptic vesicles isolated from sheep brain cortex. *Neuroscience letters* **247**, 87-90 (1998).

64 Bartholome, O. *et al.* Puzzling Out Synaptic Vesicle 2 Family Members Functions. *Frontiers in molecular neuroscience* **10**, 148, doi:10.3389/fnmol.2017.00148 (2017).

65 Buckley, K. & Kelly, R. B. Identification of a transmembrane glycoprotein specific for secretory vesicles of neural and endocrine cells. *The Journal of cell biology* **100**, 1284-1294 (1985).

66 Bajjalieh, S. M., Peterson, K., Shinghal, R. & Scheller, R. H. SV2, a brain synaptic vesicle protein homologous to bacterial transporters. *Science (New York, N.Y.)* **257**, 1271-1273 (1992).

67 Feany, M. B., Lee, S., Edwards, R. H. & Buckley, K. M. The synaptic vesicle protein SV2 is a novel type of transmembrane transporter. *Cell* **70**, 861-867 (1992).

68 Janz, R. & Sudhof, T. C. SV2C is a synaptic vesicle protein with an unusually restricted localization: anatomy of a synaptic vesicle protein family. *Neuroscience* **94**, 1279-1290 (1999).

69 Janz, R., Goda, Y., Geppert, M., Missler, M. & Sudhof, T. C. SV2A and SV2B function as redundant Ca^{2+} regulators in neurotransmitter release. *Neuron* **24**, 1003-1016 (1999).

70 Wan, Q. F. *et al.* SV2 acts via presynaptic calcium to regulate neurotransmitter release. *Neuron* **66**, 884-895, doi:10.1016/j.neuron.2010.05.010 (2010).

71 Chang, W. P. & Sudhof, T. C. SV2 renders primed synaptic vesicles competent for Ca^{2+} -induced exocytosis. *The Journal of neuroscience : the official journal of the Society for Neuroscience* **29**, 883-897, doi:10.1523/JNEUROSCI.4521-08.2009 (2009).

72 Sumiyama, K., Kawakami, K. & Yagita, K. A simple and highly efficient transgenesis method in mice with the Tol2 transposon system and cytoplasmic microinjection. *Genomics* **95**, 306-311, doi:10.1016/j.ygeno.2010.02.006 (2010).

73 Sunagawa, G. A. *et al.* Mammalian Reverse Genetics without Crossing Reveals Nr3a as a Short-Sleeper Gene. *Cell reports* **14**, 662-677, doi:10.1016/j.celrep.2015.12.052 (2016).

74 Hell, J. W. & Jahn, R. in *Cell Biology: A laboratory Handbook* 567-574 (Academic Press, 1994).

75 Palmgren, M. G. Acridine orange as a probe for measuring pH gradients across membranes: mechanism and limitations. *Analytical biochemistry* **192**, 316-321 (1991).

76 Zoccarato, F., Cavallini, L. & Alexandre, A. The pH-sensitive dye acridine orange as a tool to monitor exocytosis/endocytosis in synaptosomes. *Journal of neurochemistry* **72**, 625-633 (1999).

77 Bellocchio, E. E., Reimer, R. J., Fremeau, R. T., Jr. & Edwards, R. H. Uptake of glutamate into synaptic vesicles by an inorganic phosphate transporter. *Science (New York, N.Y.)* **289**, 957-960 (2000).

78 Hell, J. W., Maycox, P. R. & Jahn, R. Energy dependence and functional reconstitution of the gamma-aminobutyric acid carrier from synaptic vesicles. *The Journal of biological chemistry* **265**, 2111-2117 (1990).

79 Marks, P. W. & Maxfield, F. R. Preparation of solutions with free calcium concentration in the nanomolar range using 1,2-bis(o-aminophenoxy)ethane-N,N,N',N'-tetraacetic acid. *Analytical biochemistry* **193**, 61-71 (1991).

80 Egashira, Y., Takase, M. & Takamori, S. Monitoring of vacuolar-type H+ ATPase-

mediated proton influx into synaptic vesicles. *The Journal of neuroscience : the official journal of the Society for Neuroscience* **35**, 3701-3710, doi:10.1523/JNEUROSCI.4160-14.2015 (2015).

81 Egashira, Y. *et al.* Unique pH dynamics in GABAergic synaptic vesicles illuminates the mechanism and kinetics of GABA loading. *Proceedings of the National Academy of Sciences of the United States of America* **113**, 10702-10707, doi:10.1073/pnas.1604527113 (2016).

82 Jiang, M. & Chen, G. High Ca^{2+}-phosphate transfection efficiency in low-density neuronal cultures. *Nature protocols* **1**, 695-700, doi:10.1038/nprot.2006.86 (2006).

83 Mani, M. & Ryan, T. A. Live imaging of synaptic vesicle release and retrieval in dopaminergic neurons. *Frontiers in neural circuits* **3**, 3, doi:10.3389/neuro.04.003.2009 (2009).

84 Sankaranarayanan, S., De Angelis, D., Rothman, J. E. & Ryan, T. A. The use of pHluorins for optical measurements of presynaptic activity. *Biophysical journal* **79**, 2199-2208, doi:10.1016/s0006-3495(00)76468-x (2000).

85 Goncalves, P. P., Meireles, S. M., Neves, P. & Vale, M. G. Synaptic vesicle Ca^{2+}/H^{+} antiport: dependence on the proton electrochemical gradient. *Brain research. Molecular brain research* **71**, 178-184 (1999).

86 Goncalves, P. P., Meireles, S. M., Neves, P. & Vale, M. G. Methods for analysis of Ca^{2+}/H^{+} antiport activity in synaptic vesicles isolated from sheep brain cortex. *Brain research. Brain research protocols* **5**, 102-108 (2000).

87 Tsien, R. Y. New calcium indicators and buffers with high selectivity against magnesium and protons: design, synthesis, and properties of prototype structures. *Biochemistry* **19**, 2396-2404 (1980).

88 Hauschka, P. V. Analysis of nucleotide pools in animal cells. *Methods in cell biology* **7**, 361-462 (1973).

89 Plagemann, P. G. & Erbe, J. Thymidine transport by cultured Novikoff hepatoma cells and uptake by simple diffusion and relationship to incorporation into deoxyribonucleic acid. *The Journal of cell biology* **55**, 161-178 (1972).

90 Iino, M. Calcium-induced calcium release mechanism in guinea pig taenia caeci. *The Journal of general physiology* **94**, 363-383 (1989).

91 Goncalves, P. P., Meireles, S. M., Neves, P. & Vale, M. G. Ionic selectivity of the Ca^{2+}/H^{+} antiport in synaptic vesicles of sheep brain cortex. *Brain research.*

Molecular brain research **67**, 283-291 (1999).

92 Jahn, R., Schiebler, W., Ouimet, C. & Greengard, P. A 38,000-dalton membrane protein (p38) present in synaptic vesicles. *Proceedings of the National Academy of Sciences of the United States of America* **82**, 4137-4141 (1985).

93 Lynch, B. A. *et al.* The synaptic vesicle protein SV2A is the binding site for the antiepileptic drug levetiracetam. *Proceedings of the National Academy of Sciences of the United States of America* **101**, 9861-9866, doi:10.1073/pnas.0308208101 (2004).

94 Lee, J. *et al.* Exploring the interaction of SV2A with racetams using homology modelling, molecular dynamics and site-directed mutagenesis. *PloS one* **10**, e0116589, doi:10.1371/journal.pone.0116589 (2015).

95 Michelangeli, F. & East, J. M. A diversity of SERCA Ca^{2+} pump inhibitors. *Biochemical Society transactions* **39**, 789-797, doi:10.1042/BST0390789 (2011).

96 Cole, T. B., Wenzel, H. J., Kafer, K. E., Schwartzkroin, P. A. & Palmiter, R. D. Elimination of zinc from synaptic vesicles in the intact mouse brain by disruption of the ZnT3 gene. *Proceedings of the National Academy of Sciences of the United States of America* **96**, 1716-1721 (1999).

97 Palmiter, R. D., Cole, T. B., Quaife, C. J. & Findley, S. D. ZnT-3, a putative transporter of zinc into synaptic vesicles. *Proceedings of the National Academy of Sciences of the United States of America* **93**, 14934-14939 (1996).

98 Wenzel, H. J., Cole, T. B., Born, D. E., Schwartzkroin, P. A. & Palmiter, R. D. Ultrastructural localization of zinc transporter-3 (ZnT-3) to synaptic vesicle membranes within mossy fiber boutons in the hippocampus of mouse and monkey. *Proceedings of the National Academy of Sciences of the United States of America* **94**, 12676-12681 (1997).

99 Miesenbock, G., De Angelis, D. A. & Rothman, J. E. Visualizing secretion and synaptic transmission with pH-sensitive green fluorescent proteins. *Nature* **394**, 192-195, doi:10.1038/28190 (1998).

100 Mitchell, S. J. & Ryan, T. A. Syntaxin-1A is excluded from recycling synaptic vesicles at nerve terminals. *The Journal of neuroscience : the official journal of the Society for Neuroscience* **24**, 4884-4888, doi:10.1523/JNEUROSCI.0174-04.2004 (2004).

101 Schiavo, G. *et al.* Tetanus and botulinum-B neurotoxins block neurotransmitter

release by proteolytic cleavage of synaptobrevin. *Nature* **359**, 832-835, doi:10.1038/359832a0 (1992).

102 Thomas, R. C. The plasma membrane calcium ATPase (PMCA) of neurones is electroneutral and exchanges 2 H^+ for each Ca^{2+} or Ba^{2+} ion extruded. *The Journal of physiology* **587**, 315-327, doi:10.1113/jphysiol.2008.162453 (2009).

103 Carafoli, E. Calcium pump of the plasma membrane. *Physiological reviews* **71**, 129-153, doi:10.1152/physrev.1991.71.1.129 (1991).

104 Schoch, S. *et al.* SNARE function analyzed in synaptobrevin/VAMP knockout mice. *Science (New York, N.Y.)* **294**, 1117-1122, doi:10.1126/science.1064335 (2001).

105 Hicks, B. W. & Parsons, S. M. Characterization of the P-type and V-type ATPases of cholinergic synaptic vesicles and coupling of nucleotide hydrolysis to acetylcholine transport. *Journal of neurochemistry* **58**, 1211-1220 (1992).

106 Xie, X. S., Stone, D. K. & Racker, E. Purification of a vanadate-sensitive ATPase from clathrin-coated vesicles of bovine brain. *The Journal of biological chemistry* **264**, 1710-1714 (1989).

107 Blondeau, F. *et al.* Tandem MS analysis of brain clathrin-coated vesicles reveals their critical involvement in synaptic vesicle recycling. *Proceedings of the National Academy of Sciences of the United States of America* **101**, 3833-3838, doi:10.1073/pnas.0308186101 (2004).

108 Goncalves, P. P., Meireles, S. M., Neves, P. & Vale, M. G. Ca^{2+} sensitivity of synaptic vesicle dopamine, gamma-aminobutyric acid, and glutamate transport systems. *Neurochemical research* **26**, 75-81 (2001).

109 Eriksen, J. *et al.* Protons Regulate Vesicular Glutamate Transporters through an Allosteric Mechanism. *Neuron* **90**, 768-780, doi:10.1016/j.neuron.2016.03.026 (2016).

110 Juge, N., Muroyama, A., Hiasa, M., Omote, H. & Moriyama, Y. Vesicular inhibitory amino acid transporter is a Cl^-/gamma-aminobutyrate Co-transporter. *The Journal of biological chemistry* **284**, 35073-35078, doi:10.1074/jbc.M109.062414 (2009).

111 Tabb, J. S., Kish, P. E., Van Dyke, R. & Ueda, T. Glutamate transport into synaptic vesicles. Roles of membrane potential, pH gradient, and intravesicular pH. *The Journal of biological chemistry* **267**, 15412-15418 (1992).

112 Zhang, Z., Nguyen, K. T., Barrett, E. F. & David, G. Vesicular ATPase inserted into the plasma membrane of motor terminals by exocytosis alkalinizes cytosolic pH and facilitates endocytosis. *Neuron* **68**, 1097-1108, doi:10.1016/j.neuron.2010.11.035 (2010).

113 Krebs, J. The plethora of PMCA isoforms: Alternative splicing and differential expression. *Biochimica et biophysica acta* **1853**, 2018-2024, doi:10.1016/j.bbamcr.2014.12.020 (2015).

114 Kim, M. H., Korogod, N., Schneggenburger, R., Ho, W. K. & Lee, S. H. Interplay between Na^+/Ca^{2+} exchangers and mitochondria in Ca^{2+} clearance at the calyx of Held. *The Journal of neuroscience : the official journal of the Society for Neuroscience* **25**, 6057-6065, doi:10.1523/jneurosci.0454-05.2005 (2005).

115 Chen, L., Koh, D. S. & Hille, B. Dynamics of calcium clearance in mouse pancreatic beta-cells. *Diabetes* **52**, 1723-1731, doi:10.2337/diabetes.52.7.1723 (2003).

116 Madeo, M., Kovacs, A. D. & Pearce, D. A. The human synaptic vesicle protein, SV2A, functions as a galactose transporter in Saccharomyces cerevisiae. *The Journal of biological chemistry* **289**, 33066-33071, doi:10.1074/jbc.C114.584516 (2014).

117 Crowder, K. M. *et al.* Abnormal neurotransmission in mice lacking synaptic vesicle protein 2A (SV2A). *Proceedings of the National Academy of Sciences of the United States of America* **96**, 15268-15273 (1999).

118 Stafford, N., Wilson, C., Oceandy, D., Neyses, L. & Cartwright, E. J. The Plasma Membrane Calcium ATPases and Their Role as Major New Players in Human Disease. *Physiological reviews* **97**, 1089-1125, doi:10.1152/physrev.00028.2016 (2017).

119 Malmberg, C. & Maryott, A. Dielectric Constant of Water from 0° to 100° C. *Journal of Research of the National Bureau of Standards* **56**, 2641 (1956).

120 Harrison, S. M. & Bers, D. M. The effect of temperature and ionic strength on the apparent Ca-affinity of EGTA and the analogous Ca-chelators BAPTA and dibromo-BAPTA. *Biochimica et biophysica acta* **925**, 133-143 (1987).

121 Wilson, J. E. & Chin, A. Chelation of divalent cations by ATP, studied by titration calorimetry. *Analytical biochemistry* **193**, 16-19 (1991).

7. Acknowledgements

I would like to thank Prof. Dr. Shigeo Takamori not only for his invaluable support and guidance throughout this PhD project but also for sharing his enthusiasm and love for science with me.

Many thanks go to Dr. Yasunori Mori for patiently helping me face the challenges and sustain my motivation. I would like to thank him also for scientific inputs and technical supports, especially plasmid constructions and imaging experiments.

I would like to thank Dr. Yoshihiro Egashira for the assistance of data analysis and technical supports. In particular, when I was in trouble over the isolation of the synaptic vesicle fraction, he gave me sound advice about how to solve the problems.

I am grateful to my collaborator, Dr. Kenta Sumiyama for generating all SV2-deficient mice used in my thesis.

I would like to express my gratitude to Dr. Yukihiro Nakamura for his advice about the calculation of the free Ca^{2+}, and also to Dr. Tomohiro Miyasaka and Dr. Satoru Funamoto for kindly sharing the ultracentrifuge.

I would like to thank all the past and present members of Takamori laboratory for providing a nice and friendly working atmosphere, especially Dr. Isa, the skilled technician, Mrs. Takase, and the secretary, Mrs. Nagasawa.

Lastly and the most importantly, I would like to thank my family. Without their long-term support, I would have not achieved any of my goals in my life and therefore I dedicate this thesis.